

Water Resources Research

RESEARCH ARTICLE

10.1029/2019WR026101

Key Points:

- Flood deposition along bedrock-influenced anastomosed channels is preferentially initiated over topographic lows on exposed bedrock
- Vegetation succession on developing bars and islands increases erosional resistance, and captures additional sediment and organics
- Bedrock topographic lows become topographic highs (bedrock-core bars and islands) in the latter stages of sediment accumulation

Correspondence to:

D. J. Milan,
D.Milan@hull.ac.uk

Citation:

Milan, D. J., Tooth, S., & Heritage, G. L. (2020). Topographic, hydraulic, and vegetative controls on bar and island development in mixed bedrock-alluvial, multichanneled, dryland rivers. *Water Resources Research*, 56. <https://doi.org/10.1029/2019WR026101>

Received 3 AUG 2019

Accepted 11 MAR 2020

Accepted article online 16 MAR 2020

Topographic, Hydraulic, and Vegetative Controls on Bar and Island Development in Mixed Bedrock-Alluvial, Multichanneled, Dryland Rivers

D. J. Milan¹ , S. Tooth² , and G. L. Heritage³

¹Department of Geography, Geology and Environment, University of Hull, Hull, UK, ²Department of Geography and Earth Sciences, Aberystwyth University, Aberystwyth, UK, ³School of Environment and Life Sciences, Peel Building, University of Salford, Salford, UK

Abstract We investigate processes of bedrock-core bar and island development in a bedrock-influenced anastomosed reach of the Sabie River, Kruger National Park, eastern South Africa. For sites subject to alluvial stripping during an extreme flood event ($\sim 4,470\text{--}5,630\text{ m}^3\text{ s}^{-1}$) in 2012, pre-flood and post-flood aerial photographs and LiDAR data, 2-D morphodynamic simulations, and field observations reveal that the thickest surviving alluvial deposits tend to be located over bedrock topographic lows. At a simulated peak discharge ($\sim 4,500\text{ m}^3\text{ s}^{-1}$), most sediment (sand, fine gravel) is mobile but localized deposition on bedrock topographic highs is possible. At lower simulated discharges ($<1,000\text{ m}^3\text{ s}^{-1}$), topographic highs are not submerged, and deposition occurs in lower elevation areas, particularly in areas disconnected from the main channels during falling stage. Field observations suggest that in addition to discharge, rainwash between floods may redistribute sediments from bedrock topographic highs to lower elevation areas, and also highlight the critical role of vegetation colonization in bar stability, and in trapping of additional sediment and organics. These findings challenge the assumptions of preferential deposition on topographic highs that underpin previous analyses of Kruger National Park river dynamics, and are synthesized in a new conceptual model that demonstrates how initial bedrock topographic lows become topographic highs (bedrock-core bars and islands) in the latter stages of sediment accumulation. The model provides particular insight into the development of mixed bedrock-alluvial anastomosing along the Kruger National Park rivers, but similar processes of bar/island development likely occur along numerous other bedrock-influenced rivers across dryland southern Africa and farther afield.

1. Introduction

Considerable recent research attention has been given to the dynamics of sediment cover in bedrock or mixed bedrock-alluvial rivers, including in field investigations (e.g., Goode & Wohl, 2010; Hodge et al., 2011; Hodge & Hoey, 2016), laboratory flume experiments (e.g., Chatanantavet & Parker, 2008; Finnegan et al., 2007; Hodge et al., 2011; Hodge & Hoey, 2016; Johnson & Whipple, 2007), and numerical modeling studies (e.g., Huda & Small, 2014; Johnson, 2014; Sklar & Dietrich, 2004). In some settings, fluvial and wider landscape development is thought to be strongly influenced by the degree of sediment cover owing to its control on river incision rates through bedrock (Lague, 2014; Nelson & Seminara, 2011; Sklar & Dietrich, 2004). A delicate balance exists, with sediment acting both as a tool for abrasion and as a protective cover against erosion (Howard, 1994; Sklar & Dietrich, 2004). Most researchers have assumed that over long time periods a negative feedback exists, whereby enhanced bedrock erosion is counteracted by development of a protective sediment cover (e.g., Lague, 2014; Nelson & Seminara, 2011; Sklar & Dietrich, 2004). In contrast, the flume experiments of Johnson and Whipple (2007) and Finnegan et al. (2007) indicate a positive feedback mechanism, whereby the locations of sediment over the bedrock are associated with increased erosion rates. In these types of rivers, therefore, the patterns, processes, and rates of bedform, barform, and island development may be crucial controls on bedrock exposure and its longer-term susceptibility to erosion (Meshkova & Carling, 2012; Tooth & McCarthy, 2004).

Against this backdrop, clearly there is a critical need for additional field, laboratory, and numerical modeling studies of the dynamics of sediment cover in different bedrock or mixed bedrock-alluvial river styles. Southern Africa provides an opportunity to conduct such studies, for many of the rivers draining the dryland

©2020. The Authors.

This is an open access article under the terms of the Creative Commons Attribution License, which permits use, distribution and reproduction in any medium, provided the original work is properly cited.

interior of the subcontinent are characterized by bedrock “macrochannels” that commonly have incised many meters into ancient planation surfaces but have variable amounts of sediment infill. Variations in lithology, geological structure, flow regime, sediment supply, sediment cohesion, and vegetation assemblages have created morphologically diverse river styles, many of which have been characterized by extended periods of sediment accumulation on an historic time scale (Tooth, 2016; Tooth & Nanson, 2011). This has led to the development of an increasingly alluvial and vegetated set of single-thread and multichannel river styles that commonly result in decreasing exposure of the underlying bedrock (McCarthy & Tooth, 2004; Parsons et al., 2006; Rountree et al., 2000; Tooth et al., 2013; Tooth & McCarthy, 2004; van Coller et al., 1997; van Niekerk et al., 1995). Nevertheless, sediment accumulation is periodically interrupted by extensive “stripping” of alluvium and associated vegetation during large or extreme floods (e.g., Heritage et al., 2004; Milan, Heritage, Tooth, et al., 2018; Pettit & Naiman, 2006; Rountree et al., 2000, 2001; Tooth & McCarthy, 2004). Similar stripping events have been highlighted as an important driver of channel dynamics and alluvial system resetting in some Australian (Baggs Sargood et al., 2015; Nanson, 1986), Indian (Kale et al., 1996), and North American river systems (Baker, 1977; Graf, 1983; Hereford, 1984, 1993). In rivers where bedrock lies at shallow depth beneath the alluvium, stripping leads to exposure during floods, thereby facilitating further bedrock incision (e.g., Baggs Sargood et al., 2015; Heritage et al., 2014; Milan, Heritage, Entwistle, et al., 2018; Milan, Heritage, Tooth, et al., 2018).

Along many reaches of mixed bedrock-alluvial rivers in southern Africa, anastomosing (Heritage et al., 1999, 2004) or anabranching (Tooth & McCarthy, 2004) is one of the key multichannel river styles. Wide macrochannels incised in bedrock host multiple smaller channels that divide and rejoin around bedrock-influenced bars and islands. A fundamental morphological unit in these river styles is the bedrock-core bar, which is defined as a macroscale depositional feature, typically 10–50 m in length, that is composed of an outer shell of alluvium deposited around a bedrock topographic high and is commonly colonized by vegetation (van Coller et al., 1997; van Niekerk et al., 1995). Bedrock-core bars are initiated by sediment deposition that occurs on exposed bedrock in the channel bed. Deposition is aided by the growth of pioneering vegetation such as *Bretonadia salicina* (commonly known as Matumi or Mingerhout), which often establishes in fissures on bedrock outcrop, and also by the development of reedbeds (van Niekerk et al., 1995). The location of individual bedrock-core bars remains fixed but they may grow vertically, laterally, and longitudinally through ongoing sedimentation and vegetation colonization, with neighboring bars locally coalescing to form the larger, vegetated islands around which many channels divide and rejoin (van Niekerk et al., 1995; cf. Tooth & McCarthy, 2004). Similar to many bedrock-influenced, single-thread or braided river styles (van Niekerk et al., 1995), these anastomosing/anabranching river dynamics are largely controlled by stripping of alluvium and vegetation during large or extreme events, with intervening building phases enabling sediment accumulation and vegetation re-establishment (Milan, Heritage, Tooth, et al., 2018). For the mixed bedrock-alluvial rivers in the Kruger National Park (KNP), eastern South Africa, van Niekerk et al.’s (1999) conceptual model assumes that topographic lows remain sediment free while near-uniform, ubiquitous sediment deposition begins on bedrock topographic highs during peak and waning flow stages, and that subsequent vegetation colonization on these highs promotes additional deposition. A preliminary study of the Olifants River (Milan, Heritage, Entwistle, et al., 2018) has questioned this assumption of preferential deposition on topographic highs but additional field and modeling evidence is needed for a more rigorous examination. Obtaining field data from the KNP rivers and other similar riparian environments can be difficult, however, as the periods of significant sediment accumulation that follow extensive stripping events tend to be erratic in time and space. In the KNP, additional challenges are posed by the large scale of many macrochannels (many hundreds of meters wide), locally dense vegetation, and the presence of dangerous animals.

With recent developments in data acquisition (e.g., aerial LiDAR) and numerical modeling, there is an opportunity to circumvent many of these challenges (Entwistle et al., 2018; Milan & Heritage, 2012) by undertaking spatially extensive yet locally detailed investigations of sediment dynamics and associated bar, island, and channel development. In this paper, we investigate the controls on bedrock-core bar and island development in a bedrock-influenced, anastomosed reach of the Sabie River (Figure 1a). The Sabie River is one of several large (>100 km long) rivers in the KNP that are subjected to episodic cyclone-driven, large floods (defined here as peak discharges $1,000\text{--}4,000\text{ m}^3\text{ s}^{-1}$) or extreme floods (> $4,000\text{ m}^3\text{ s}^{-1}$), most recently in February 2000 and January 2012 (Heritage et al., 2004, 2019; Knight &

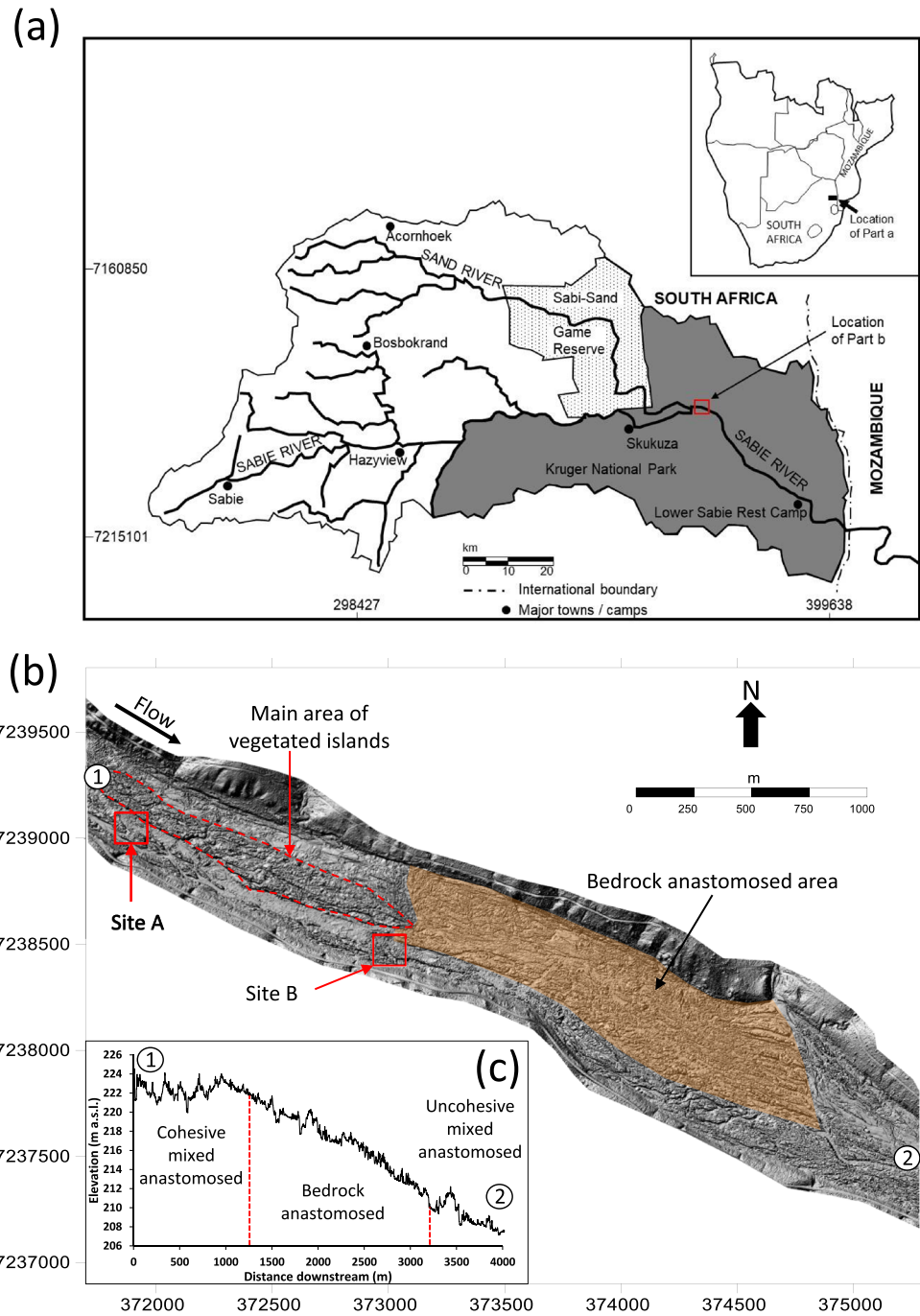


Figure 1. (a) The Sabie River catchment, eastern South Africa, showing the location of the study reach in the southern part of the Kruger National Park (KNP; dark shaded area). From the northern edge of the Sabie catchment, the KNP extends ~300 km northward along the South Africa-Mozambique border, and is traversed by many other rivers with similar characteristics to the Sabie. (b) LiDAR bare earth DEM for the study reach, which comprises sections with mixed bedrock-alluvial anastomosed (upstream, downstream) and bedrock anastomosed (midstream) channel types (see part c). The coordinate system is WGS84 UTM36S. Sites A and B (red boxed areas) show the locations for erosion depth and sedimentation thickness analyses (Figures 5 and 6). (c) Long-profile for the study reach taken along the centerline of the macrochannel between points 1 and 2 (see part b), with the transitions between the different channel types demarcated by the vertical red dashed lines.

Evans, 2017; Milan, Heritage, Tooth, et al., 2018; Smithers et al., 2001). Individually and collectively, these recent floods led to extensive stripping of alluvium and vegetation, locally revealing the underlying bedrock template (Milan, Heritage, Entwistle, et al., 2018; Milan, Heritage, Tooth, et al., 2018), but subsequent to the 2012 floods, the early stages of sediment accumulation and vegetation re-establishment have occurred. The aims of the paper are to (1) use pre-flood and post-flood aerial orthophotography and LiDAR data to map the spatial patterns of erosion and deposition resulting from the 2012 floods; (2) use two-dimensional (2-D) morphodynamic simulations to investigate topographic and hydraulic controls upon erosional and depositional patterns, with a particular focus on identifying and explaining deposition on the bedrock template; and (3) synthesize these findings with field observations of sediment redistribution and vegetation colonization in a new conceptual model of bedrock-core bar and island development.

2. Study Location

2.1. Regional Setting

The Sabie River drains a 7,096-km² catchment (Figure 1a), rising in the rugged Drakensberg to the west (~1,600 m above sea level) and descending rapidly onto the lower relief Lowveld (~400 m above sea level) and Lebombo zones (~200 m above sea level) farther east. Rainfall occurs mainly in the austral summer (November through March) and is highest in the headwaters (2,000 mm a⁻¹), declining rapidly eastward toward the South Africa-Mozambique border (450 mm a⁻¹). Flow gauge records for the middle Sabie River only extend back to the mid-1980s (Heritage et al., 2019) but demonstrate that the flow regime is highly seasonal, being characterized by austral winter low flows (generally <50 m³ s⁻¹) and summer floods that once every few years are in the 500–1,000-m³ s⁻¹ range (defined here as moderate floods). Occasionally, high-intensity rainfall events (>100 mm/day) result from the tracking of cyclones inland, and floods are in the 1,000–4,000-m³ s⁻¹ range (defined here as large floods) or exceed 4,000 m³ s⁻¹ (defined here as extreme floods; Eden, 1937; Heritage et al., 2019; Milan, Heritage, Tooth, et al., 2018).

Cyclone-driven, extreme floods occurred both in February 2000 and January 2012, with peak discharges on the Sabie River estimated at ~6,000–7,000 and ~4,470–5,630 m³ s⁻¹, respectively (Heritage et al., 2004, 2019; Milan, Heritage, Tooth, et al., 2018). Based upon rain gauge records from 1945, Smithers et al. (2001) estimated the 2000 Cyclone Eline event to have led to rainfall with return periods in excess of 200 years in parts of the upper and middle catchment. The magnitudes and probabilities of the associated floods varied throughout the catchment but from rainfall-runoff modeling, floods in most parts of the catchment were estimated to have return periods greater than 50 years (Smithers et al., 2001). Yet just 12 years later, Cyclone Dando led to more heavy rainfall and flooding (Fitchett et al., 2016). On the Sabie River, the 2012 floods were not as large as the 2000 floods but nevertheless also resulted in significant erosion and deposition (Milan, Heritage, Tooth, et al., 2018). In historical context, the close temporal spacing of these two flood events is unusual but could be explained by the mounting evidence that climate change in eastern southern Africa may be driving an increased frequency of cyclone-generated extreme events in eastern South Africa (Fitchett & Grab, 2014) and is resulting in increased rainfall during wet seasons (MacFadyen et al., 2018). The possible impacts of these climate-driven changes upon the KNP rivers has been conceptualized by Milan, Heritage, Tooth, et al. (2018) for two different initial starting states. An increasing frequency of large or extreme floods will likely initiate stripping in more alluvial reaches and thus lead to greater bedrock exposure, and will maintain widespread bedrock exposure in bedrock reaches. For both alluvial and bedrock reaches, however, the impacts of such changes in flood magnitude and frequency are likely to be spatially nonuniform and dependent on flood sequencing. Uncohesive sediments may be deposited during falling stage on exposed bedrock surfaces or during intervening lower magnitude floods (Milan, Heritage, Tooth, et al., 2018), so for the more alluvial reaches, partial or full recovery to pre-flood starting states may still occur. Among national park managers, there is concern regarding the potential impacts of these channel changes on associated aquatic and riparian ecosystems.

In terms of flow regime and morphology, the Sabie River is similar to many other rivers located farther north in the KNP, including large rivers such as the Letaba and Olifants (Heritage et al., 2019; Milan, Heritage, Entwistle, et al., 2018; Moon & Heritage, 2001). In its middle reaches, the Sabie River is characterized by a macrochannel that has incised ~5–10 m into various sedimentary, metamorphic, and intrusive and extrusive igneous lithologies (Heritage et al., 1999). Along these middle reaches, lithological changes result in

frequent, abrupt changes in macrochannel slope and associated sediment deposition patterns, leading to diverse channel types that include alluvial single-thread and braided channels, and bedrock-influenced anastomosed and pool-rapid channels (van Niekerk et al., 1995). In previous channel-type classifications of the KNP rivers (e.g., Heritage et al., 1999), the prefix “mixed” has been used as shorthand to refer to “mixed bedrock-alluvial” channels, and a distinction has been made between uncohesive mixed (dominantly mobile sand and fine gravel) and cohesive mixed (higher clay-silt proportion) channel types (Broadhurst et al., 1997). For brevity and consistency with earlier work, this terminology and distinction is adopted hereafter.

Although water abstractions have impacted the winter low-flow regime, the larger summer flood flows are less influenced, and the Sabie River remains unaffected by engineering structures or other human activities over considerable lengths within the KNP. As such, the middle reaches provide near-pristine sites for investigating the interactions between sediment dynamics, flow hydraulics, and vegetation growth that are involved in the development of bars and islands around which the mixed anastomosing channels divide and rejoin.

2.2. Study Reach

This study focuses on an ~4-km-long reach of the Sabie River within the KNP (Figures 1b and 1c). In this reach, macrochannel slopes range from ~0.0012 to 0.05 m m⁻¹ (reach-average slope ~0.004 m m⁻¹) and macrochannel width ranges from 400 to 600 m. This reach formed part of the longer (50 km) reach investigated by Milan, Heritage, Tooth, et al. (2018) in their study of the erosional, depositional, and vegetation changes resulting from the individual and synergistic impacts of the 2000 and 2012 extreme floods. This reach was chosen for detailed study because the macrochannel hosts different anastomosing channel types in close proximity, including cohesive and uncohesive mixed anastomosed types (upstream and downstream) and bedrock anastomosed types (midstream; Figures 1b, 1c, 2a, and 2b). Depending on the degree of alluvial cover that survived the 2012 extreme floods, all of these anastomosed channel types had depositional units including bedrock-core bars and islands (van Coller et al., 1997). In this shorter study reach, we investigated the sediment thicknesses characteristic of bedrock-core bars and were able to run computationally intensive morphodynamic simulations to investigate the controls on deposition over an exposed bedrock template. The smaller sites selected for the sediment thickness investigations (Figure 1b, sites A and B) were examples of where stripping of vegetation and alluvium had taken place during the 2012 event, as identified from interrogation of available 2004 and 2012 aerial photographs (see below).

The study reach is situated approximately 2 km downstream of the Sand River confluence. Owing to the granitic lithologies that underlie much of the Sabie and Sand river catchments, the dominant weathering products and associated river sediment loads comprise sand and fine gravel. Heavy rainfall from Cyclone Dando impacted the whole of the KNP, resulting in severe flooding in both the Sand and Sabie catchments. During the floods, the Sand River supplied large volumes of sediment to the Sabie, leading to widespread deposition along the north bank of the Sabie for the first few kilometers downstream of the confluence (Milan, Heritage, Tooth, et al., 2018).

3. Methods

This study used a combination of aerial LiDAR data and orthophotography analyses, field surveys and observations, and 2-D morphodynamic simulations, as detailed below.

3.1. Aerial LiDAR Data and Orthophotography Analyses

Following the Cyclone Dando floods, aerial LiDAR data and orthophotography were obtained on 30 May 2012 for a 50-km reach of the Sabie River in the KNP (Milan, Heritage, & Tooth, 2018). Southern Mapping Geospatial surveyed the river using an Opetch Orion 206 LiDAR, and a Rollei AIC with a 60-megapixel P65+ Phase One digital CCD, flown from a Cessna 206 at 1,100-m altitude. This was compared to previous LiDAR data and aerial photography obtained in 2004 following the 2000 extreme floods. Point density for the 2004 LiDAR survey was lower (46 pts m⁻²) compared to the 2012 LiDAR survey (409 pts m⁻²) but this was still considered sufficient to produce a high-quality DEM (in the sense of Heritage et al., 2009). Both the 2004 and 2012 LiDAR surveys were conducted at low flow, as confirmed by coincident aerial photos and ground surveys (see below), so key morphological units (e.g., surviving bars, islands—see Figures 2a and 2b) and large areas of bedrock template (e.g., orange shaded area in Figure 1b) were exposed. We gridded the

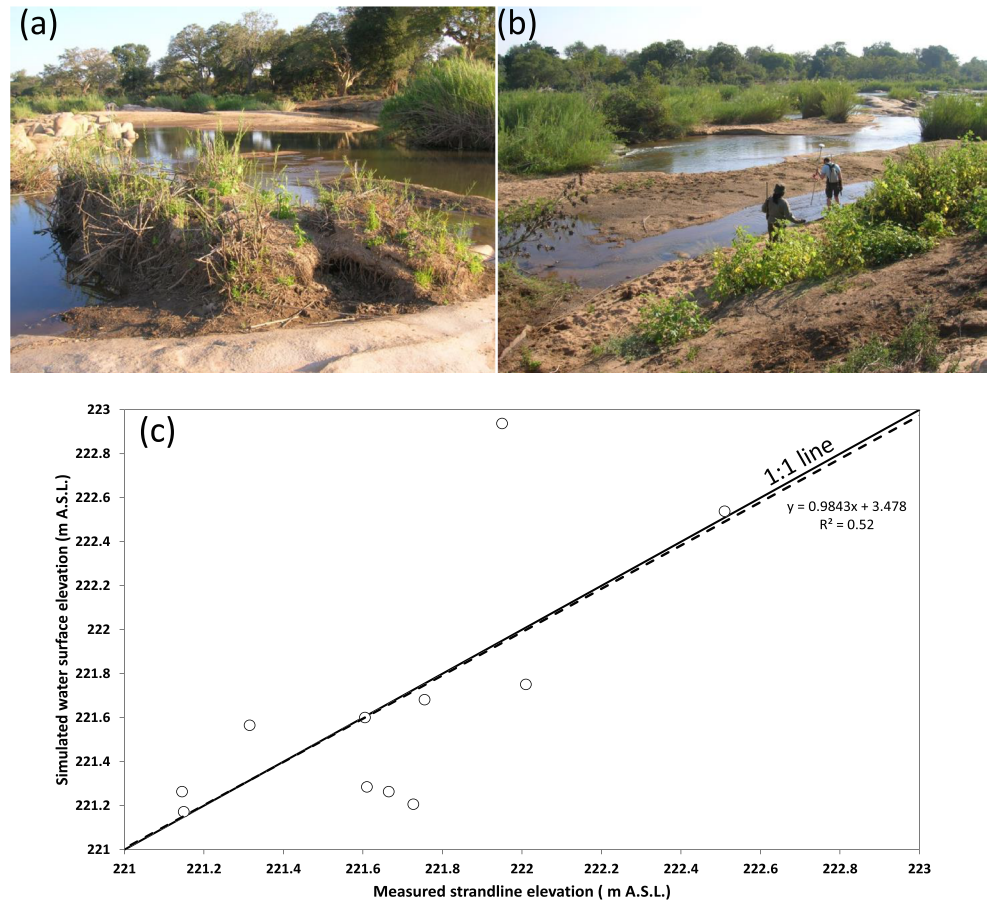


Figure 2. (a) View of the upstream part of the study reach (flow direction toward camera) illustrating remnant sediments atop bedrock. These sediments are from bedrock-core bars and islands that were partially stripped during the 2012 floods. (b) View of the mixed anastomosed channel type in the upstream part of the study reach (flow direction away from camera toward the top right) showing areas of mobile sand and fine gravel (foreground), vegetated bars and islands (middle and far distance), and areas of bedrock outcrop (far distance, top right). (c) Comparison of simulated water surface elevations versus dGPS surveyed strandlines, located in an ~250-m-long section located near the upstream end of the study reach.

LiDAR data, stripped of vegetation, at 1 m to create DEMs, using triangulation with linear interpolation to cover areas with low or no returns such as parts of the channel beds that were submerged at low flow. The DEMs were then differenced to highlight spatial patterns of erosion and deposition (in the sense of Milan et al., 2007) that could be attributed largely to the influence of the 2012 floods (see Milan, Heritage, Tooth, et al., 2018).

3.2. Field Surveys and Observations

In late May 2012, field surveys were undertaken at the same time as the LiDAR surveys for a number of sites along a 50-km reach of the middle Sabie River, including in the study reach, as well as along similarly long reaches of other KNP rivers. The elevations of strandlines created by the preceding January extreme floods were measured through dGPS survey, and used in conjunction with the aerial LiDAR imagery to estimate peak discharges and validate 2-D flow simulations conducted for the full 50 km of the middle Sabie River (see Milan, Heritage, Tooth, et al., 2018; Heritage et al., 2019). These previous 2-D flow simulations provide broader context for the new morphodynamic simulations reported in this paper (see below). Additional field observations provided qualitative insights into the topographic, hydraulic, and vegetative factors influencing local sediment reworking in the months following the 2012 floods.

3.3. The 2-D Morphodynamic Simulations

To investigate hydraulic and sediment transport processes in the study reach (Figure 1b), we undertook 2-D morphodynamic modeling using the CAESAR-Lisflood code (Coulthard et al., 2013). The aim of the simulations was not to try and replicate the impacts of the Cyclone Dando floods but rather to use the outputs in an exploratory fashion, focusing particularly on the topographic and hydraulic controls on deposition over a stripped bedrock template. Any insights gained are pertinent in view of the possible trends toward more widespread stripping and greater bedrock exposure that may occur along the KNP rivers with increasing flood magnitude and frequency, especially for improving understanding of potential trajectories of river recovery in intervening lower magnitude floods (section 2.1). A 5-m resolution DEM was employed in CAESAR-Lisflood in order to ensure that run times were manageable through to model convergence. The simulation run length was 52 hr, with a flood hydrograph that peaked at $\sim 4,500 \text{ m}^3 \text{ s}^{-1}$ at 7 hr, receded to $\sim 190 \text{ m}^3 \text{ s}^{-1}$ at 29 hr, and then rose again slightly with a smaller peak of $\sim 410 \text{ m}^3 \text{ s}^{-1}$ at 33 hr. The peak discharge at 7 hr is within the lower end of the peak discharge range ($\sim 4,470\text{--}5,630 \text{ m}^3 \text{ s}^{-1}$) reported for the 2012 floods on the Sabie (Heritage et al., 2019), as is consistent with the location of the study reach near the upper end of the 50-km-long surveyed reach. Indeed, water surface elevations for the peak discharge of the simulation demonstrate good agreement with strandline elevations obtained from the study reach using dGPS (Figure 2c). Maximum deviations of $\sim 0.9 \text{ m}$ from the 1:1 line can be explained by the fact that at many locations, elevation differences between the top and bottom of individual strandlines ranged over 1–2 m of elevation, and multiple strandlines may have resulted from pulsing on the rising or falling limb of the flood hydrographs (see also Heritage et al., 2019). Bedload in the model was predominantly sand and fine gravel, with a D_{50} of 5 mm (after Broadhurst et al., 1997; Heritage & van Niekerk, 1995). The model was run on the bare earth DEM with a Manning's "n" of 0.04. A uniform roughness value was deemed appropriate to represent the grain effect, with the topographic variation in the model capturing the variability in form roughness (see Heritage et al., 2019). Depth-averaged flow velocity was calculated using Manning's equation and sediment transport was derived from the velocity (Coulthard et al., 2013), using Wilcock and Crowe's (2003) sediment transport equation for mixed sediment sizes. The resistant exposed bedrock section, identified through interrogation of aerial images, was built into the model as a solid block flush with the surface of the DEM in the bedrock anastomosed (orange shaded) area shown in Figure 1b, with the bedrock positioned underneath the more alluvial areas upstream and downstream. This meant that sediment could only be eroded from the more alluvial areas, and this sediment was then recirculated in the model. As noted in section 3.1, bathymetric data from LiDAR were unavailable for submerged areas in the main channels, but the ground surveys showed that flows were typically shallow ($<0.5 \text{ m}$) in the bedrock anastomosed area and commonly only slightly deeper ($<1.5 \text{ m}$) in the more alluvial reaches upstream and downstream. In the DEM, these areas were filled using triangulation with linear interpolation. Overall, given the vastly greater depths that are generated in the macrochannel around the peak of large or extreme floods (up to $\sim 6 \text{ m}$), the omission of greater depth details in the model is not likely to impact significantly on the results, particularly as most attention was focused upon depositional patterns and sediment thicknesses across the exposed bedrock areas of the macrochannel that are well represented in the model.

4. Results

In the following sections, first we focus on simulated peak flow hydraulics and reach-scale erosion and deposition patterns resulting from the 2012 floods (section 4.1). Second, we explore patterns of eroded sediment thicknesses at two smaller sites (Figure 1b, sites A and B, and section 4.2). Third, we present the results from the new morphodynamic simulations, focusing upon geomorphic responses including deposition thicknesses over previously exposed areas of bedrock (section 4.3). Fourth, we explore the relationships between deposition thicknesses and flow hydraulics (velocity) and between deposition thicknesses and topography (sections 4.4 and 4.5). These results are then integrated with field observations, providing the basis for interpretation of the topographic, hydraulic, and vegetative controls on bedrock-core bar and island development (section 5).

4.1. Simulated Peak Flood Hydraulics and Geomorphic Responses to the 2012 Floods

Figure 3 shows the depth-averaged velocity distributions for the simulated $\sim 4,500\text{-m}^3 \text{ s}^{-1}$ flow, and the patterns of erosion and deposition that occurred in the study reach as a result of the 2012 extreme floods.

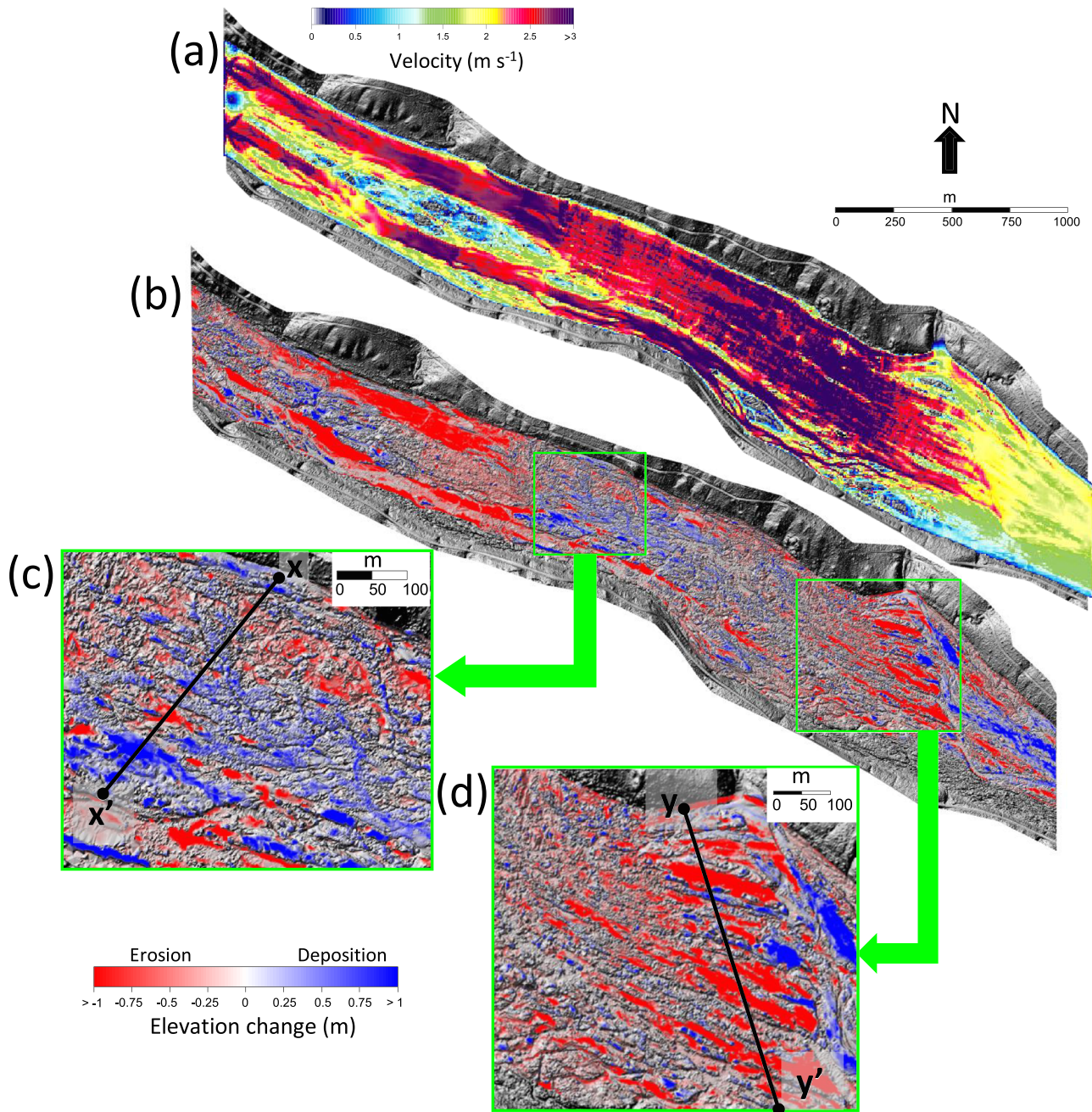


Figure 3. (a) The 2-D hydraulic simulation for a peak discharge of $\sim 4,500 \text{ m}^3 \text{ s}^{-1}$, showing spatial patterns of depth-averaged velocity. (b) DEM of Difference (DoD) showing spatial patterns of erosion and deposition resulting from the 2012 extreme floods. Particularly pronounced erosion occurred in the anabranches on either side of the main area of alluvial, vegetated islands in the upstream part of the reach. (c) Close-up of an area of net deposition, showing a dominance of deposition in topographic lows. For cross profile $x-x'$, which shows morphological changes between 2004 and 2012, see Figure 4a. (d) Close-up of an area of net erosion, much of which appears to be associated with bedrock topographic highs. For cross profile $y-y'$, which shows morphological changes between 2004 and 2012, see Figure 4b.

Simulated peak flow velocities widely exceed 2.5 m s^{-1} (Figure 3a), and the DEM of Difference (DoD) shows areas of both erosion and deposition (Figure 3b). Following spatial error filtering (e.g., Heritage et al., 2009; Milan et al., 2011), the DoD reveals overall net erosion of $\sim 418,000 \text{ m}^3$ ($\sim 23 \text{ mm m}^{-2}$).

The upstream 1.25 km of the study reach is characterized by the cohesive mixed anastomosed channel type and has a large area of vegetated islands in the center of the macrochannel (see the stippled polygon in

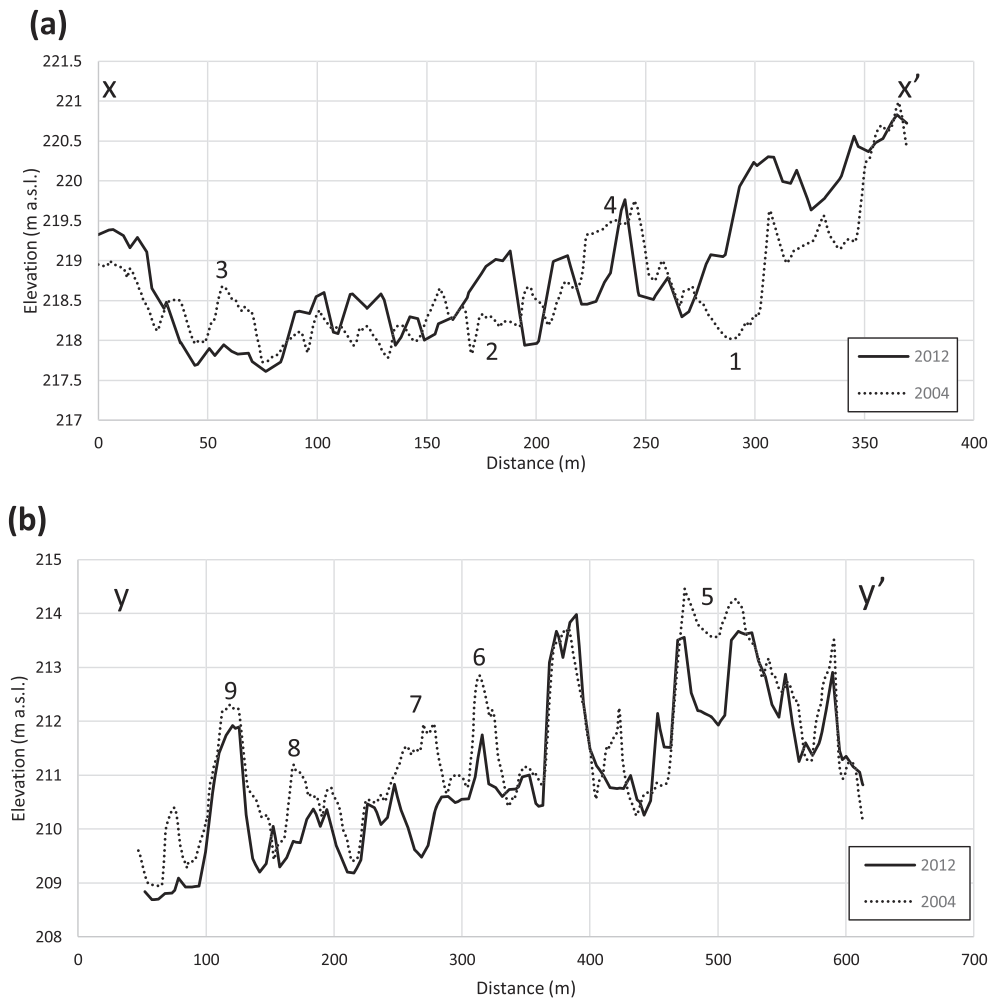


Figure 4. Cross profiles demonstrating morphological changes between 2004 and 2012, as derived from the LiDAR DoD. (a) Cross profile $x-x'$ taken from the upstream end of the bedrock anastomosed section (see Figure 3c for location). (b) Cross profile $y-y'$ taken from the downstream end of the bedrock anastomosed section (see Figure 3d for location).

Figure 1b). This area of islands remained largely intact during the 2012 floods, albeit with evidence of some deposition at the upstream end of the area and erosion at the downstream end (Figure 3b). The simulated velocity distributions (Figure 3a) show that some of the lowest velocities (typically $<0.5 \text{ m s}^{-1}$) occurred at the upstream end of the area of islands and over the top of the islands during the flood. By contrast, significant erosion occurred in the main anabranches on either side of the area of islands (Figure 3b), likely reflecting the extensive zones of high-velocity flow ($>2.5 \text{ m s}^{-1}$) evident in the simulation (Figure 3a).

The bedrock anastomosed section farther downstream shows a dominance of deposition upstream and more widespread erosion downstream (Figure 3b). Despite the generally high simulated velocities in this section (Figure 3a), the areas of deposition may reflect a locally high sediment supply from the eroding anabranches upstream, with erosion occurring farther downstream in areas with lower sediment supply. In this bedrock anastomosed section, closer inspection of the DoD reveals a general tendency for erosion of topographic highs and deposition in topographic lows (Figures 3c and 3d). Cross profiles taken from the upstream (Figure 4a) and downstream (Figure 4b) part of the bedrock anastomosed section highlight these differences in morphological response. For example, in the upstream cross profile $x-x'$, topographic lows labeled 1 and 2 both experienced up to $\sim 2 \text{ m}$ of deposition, whereas topographic highs were either lowered (3) or narrowed (4) by erosion (Figure 4a). The downstream cross section $y-y'$ shows a dominance of erosion, with most of the topographic highs (5, 6, 7, 8, 9) experiencing up to $\sim 2 \text{ m}$ of lowering or tens of meters of narrowing (Figure 4b).

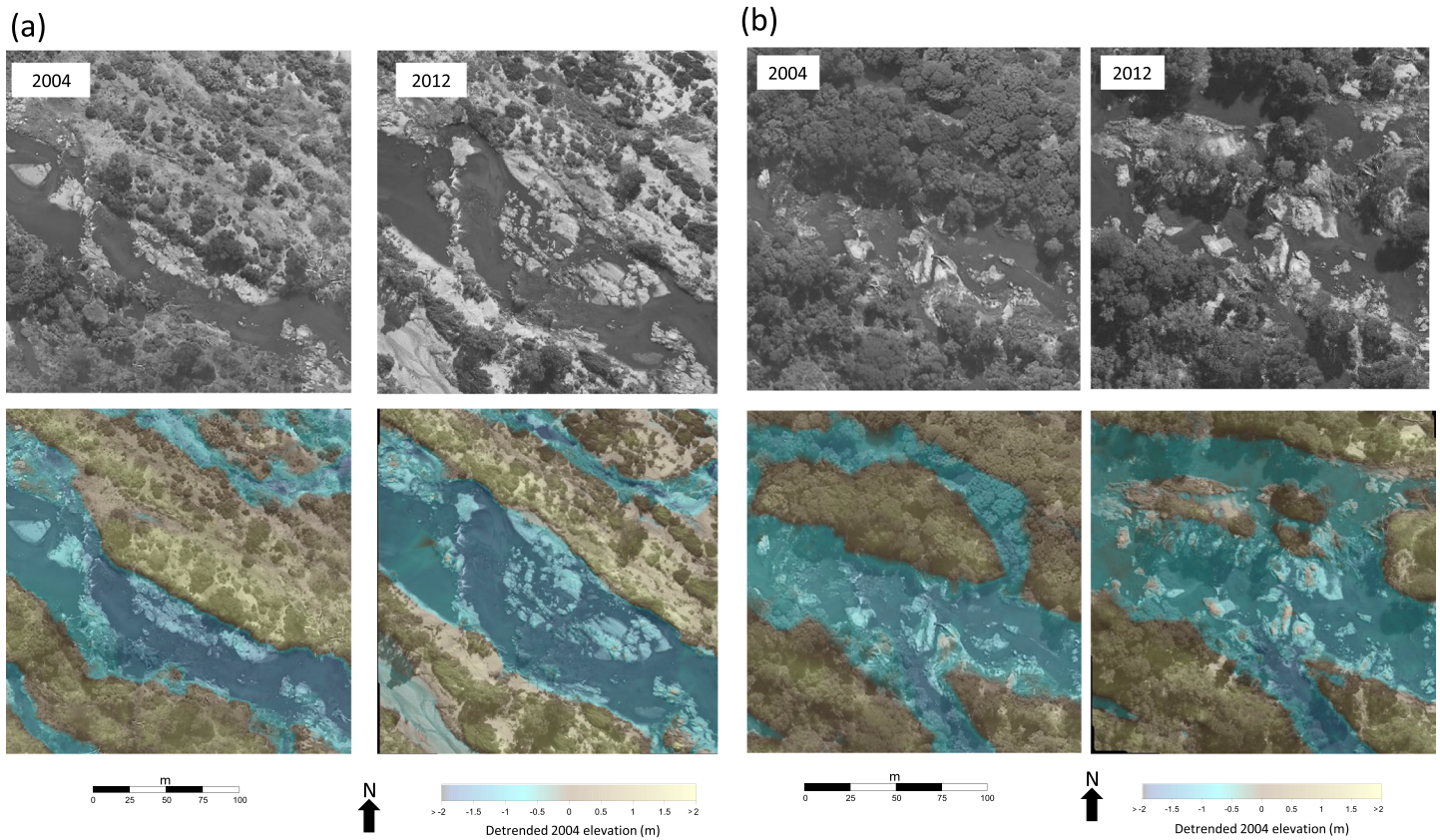


Figure 5. Aerial photographs for (a) site A and (b) site B (for locations, see Figure 1b). Both images show a dominantly alluvial, vegetated state in 2004 (top left), and a partially stripped, less vegetated state following the January 2012 extreme floods (top right). In both (a) and (b), the bottom left and bottom right figures show the corresponding detrended DEM overlain on the aerial photographs.

4.2. Sediment Thicknesses Derived From Analysis of LiDAR Data

To investigate the association between eroded sediment thicknesses and topography in greater detail, further analysis focused on two bedrock-core bars (Figure 1b, sites A and B). For site A, the evidence shows that a substantial area of sediment and vegetation was removed during the 2012 floods (Figure 5a), whereas for site B some residual patches of mature vegetation appear to have survived the floods (Figure 5b).

The DEMs from 2004 and 2012 for the two sites were detrended to remove the regional slope and reveal local topographic highs and lows. In the bottom parts of Figures 5a and 5b, the detrended DEMs are overlain on the aerial photographs and highlight that most of the still vegetated areas are associated with topographic highs. The 2004 and 2012 DEMs from the two sites were differenced to produce DoDs. For an area of significant erosion at each of the sites, the DoDs were digitized to determine local eroded sediment thicknesses. These eroded sediment thicknesses were then classed into thickness categories and overlain on the detrended 2004 DEM. Figure 6 shows that the greatest original sediment thicknesses were associated with the initial local topographic highs, namely, fully developed bedrock-core bars. Hence, when sediment thickness is plotted against the surface elevations of the fully developed bedrock-core bar using the 2004 LiDAR data, a positive relationship is apparent (Figures 7a and 7b). These data show that the topographic highs on a bedrock-core bar have the thickest sediment. By contrast, when eroded sediment thickness data are plotted against detrended elevations using the 2012 LiDAR data (Figures 7c and 7d), the greatest sediment thicknesses are associated with local topographic lows (“hollows”) on the bedrock template. This finding suggests that initial topographic lows on a stripped bedrock anastomosed template may eventually become topographic highs as the system becomes more alluvial and transitions toward an uncohesive or cohesive mixed anastomosed channel type, especially if this deposition is coupled with vegetation re-establishment (see section 5).

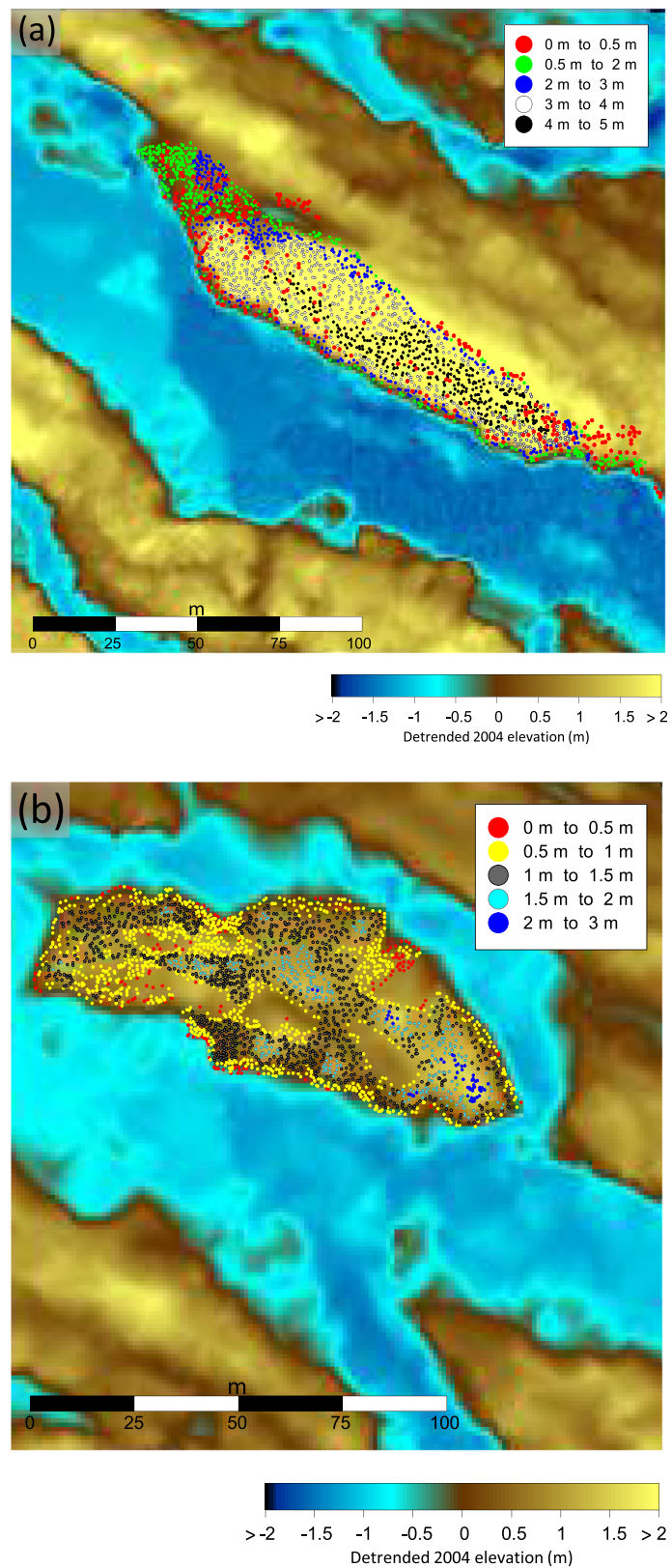


Figure 6. Classed post maps showing eroded sediment thickness (as colored dots) overlain on the detrended 2004 DEM for (a) part of site A and (b) part of site B (for locations of sites A and B, see Figure 1b). Greater eroded sediment thicknesses coincide with topographic highs on a fully developed bedrock-core bar (2004 state).

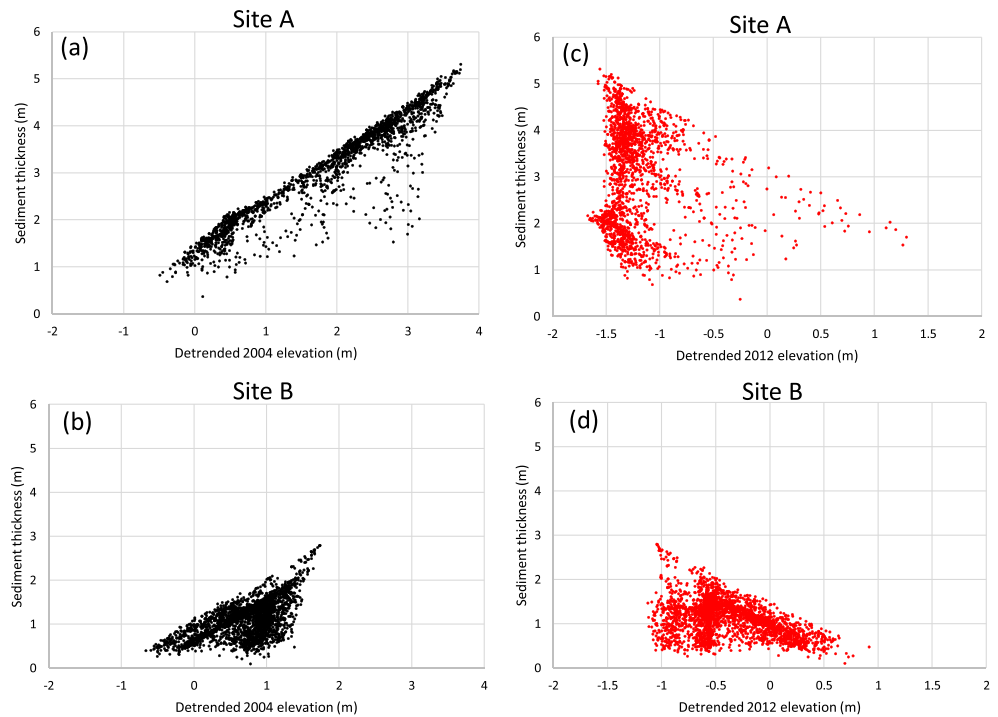


Figure 7. Sediment thicknesses for the areas of bedrock-core bars shown in Figure 6 versus (a and b) detrended 2004 elevations and (c and d) detrended 2012 elevations. The 2004 data (a and b) show that prior to the 2012 extreme floods, the thickest sediments were associated with the positive topography formed by the bedrock-core bars. The 2012 images (c and d) show that following the floods, thicker sediments are now associated with negative topography, namely, bedrock topographic lows (hollows).

4.3. The 2-D Morphodynamic Simulations: Spatial Patterns of Geomorphic Response

To investigate further the topographic and hydraulic controls on patterns of erosion, deposition, and channel development, particularly over a stripped bedrock anastomosed template, we undertook additional 2-D morphodynamic simulations. Figure 8 shows the spatial distribution of depth-averaged spatial velocity and the associated erosional and depositional patterns in the study reach at various stages during the simulated 52-hr flood with a peak discharge of $\sim 4,500 \text{ m}^3 \text{ s}^{-1}$. For all stages, spatially variable velocity distributions are evident throughout the study reach, with large areas exposed above the water surface during the lower discharges (Figure 8a). In the cohesive mixed anastomosed section at the upstream end of the reach, as discharge increases there is some evidence of velocity reversals in the main anabranches laterally adjacent to the main area of alluvial islands. At low flow, the main anabranches tend to have velocities $< 1 \text{ m s}^{-1}$, compared with areas of higher velocities both immediately upstream and downstream. Conversely, at the flood peak, some of the highest velocities ($> 3 \text{ m s}^{-1}$) are in the anabranches laterally adjacent to the main area of islands, and areas of lower velocities are found both immediately upstream and downstream (Figure 8a). This peak flood velocity pattern helps to explain the spatial distribution of erosion and deposition resulting from the 2012 floods (Figure 3b), with significant erosion occurring in the main anabranches where flow competence probably exceeded sediment supply, and more deposition occurring slightly downstream where sediment supply probably exceeded flow competence.

The bedrock anastomosed section in the midstream part of the study reach appears as a zone of relatively high-velocity flow over most of the simulated flood hydrograph, with peak velocities in excess of 5 m s^{-1} at flows of $\sim 4,500 \text{ m}^3 \text{ s}^{-1}$ (Figure 8a). Nonetheless, the morphodynamic simulations show that some deposition occurs in this bedrock anastomosed section (Figure 8b). Initially, this appears as an elongate linear ribbon almost in line with the tail of the main area of alluvial islands upstream (see Figure 8b; 7 hr), which later becomes dissected. Figure 9 shows the bedrock anastomosed section in greater detail after the full 52-hr simulation, illustrating that some deposition also occurs on the bedrock template on the waning limb of

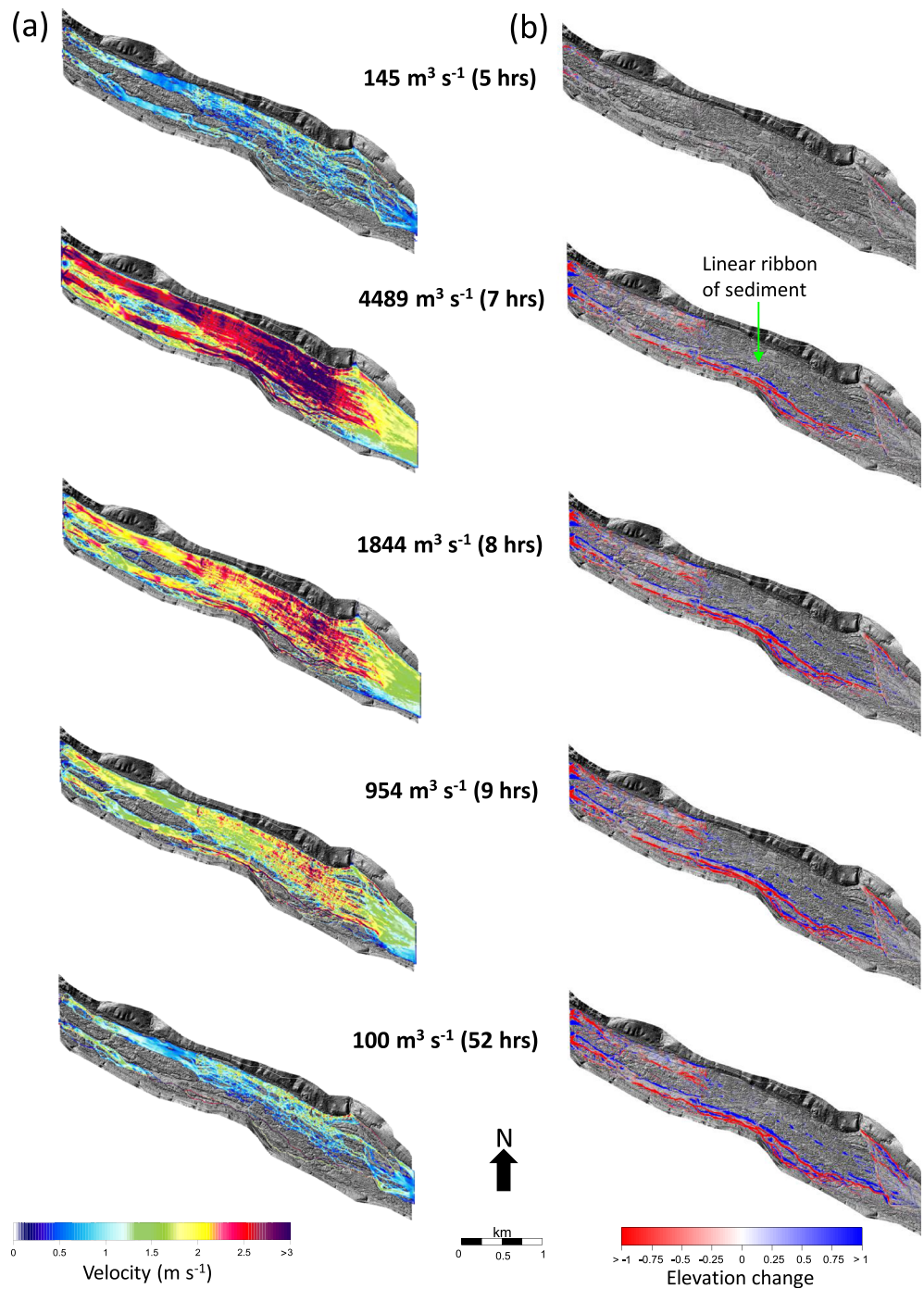


Figure 8. (a) Depth-averaged velocity distributions at different discharges over a 52-hr hydrograph with a flood peak of $\sim 4,500 \text{ m}^3 \text{ s}^{-1}$. (b) Simulated erosion and deposition patterns at different discharges over the 52-hr hydrograph, showing how most erosion and deposition occurs in the mixed anastomosed sections upstream and downstream of the bedrock anastomosed section.

the hydrograph, including on some topographic highs, but particularly at major breaks of slope and in bedrock topographic lows. For instance, at the upstream end of the bedrock anastomosed section, a long profile (Figure 9b; $z-z'$) reveals how deposits up to 1.6 m thick tend to correlate with low points on the underlying bedrock template, some of which are in the lee of bedrock topographic highs (Figure 9c).

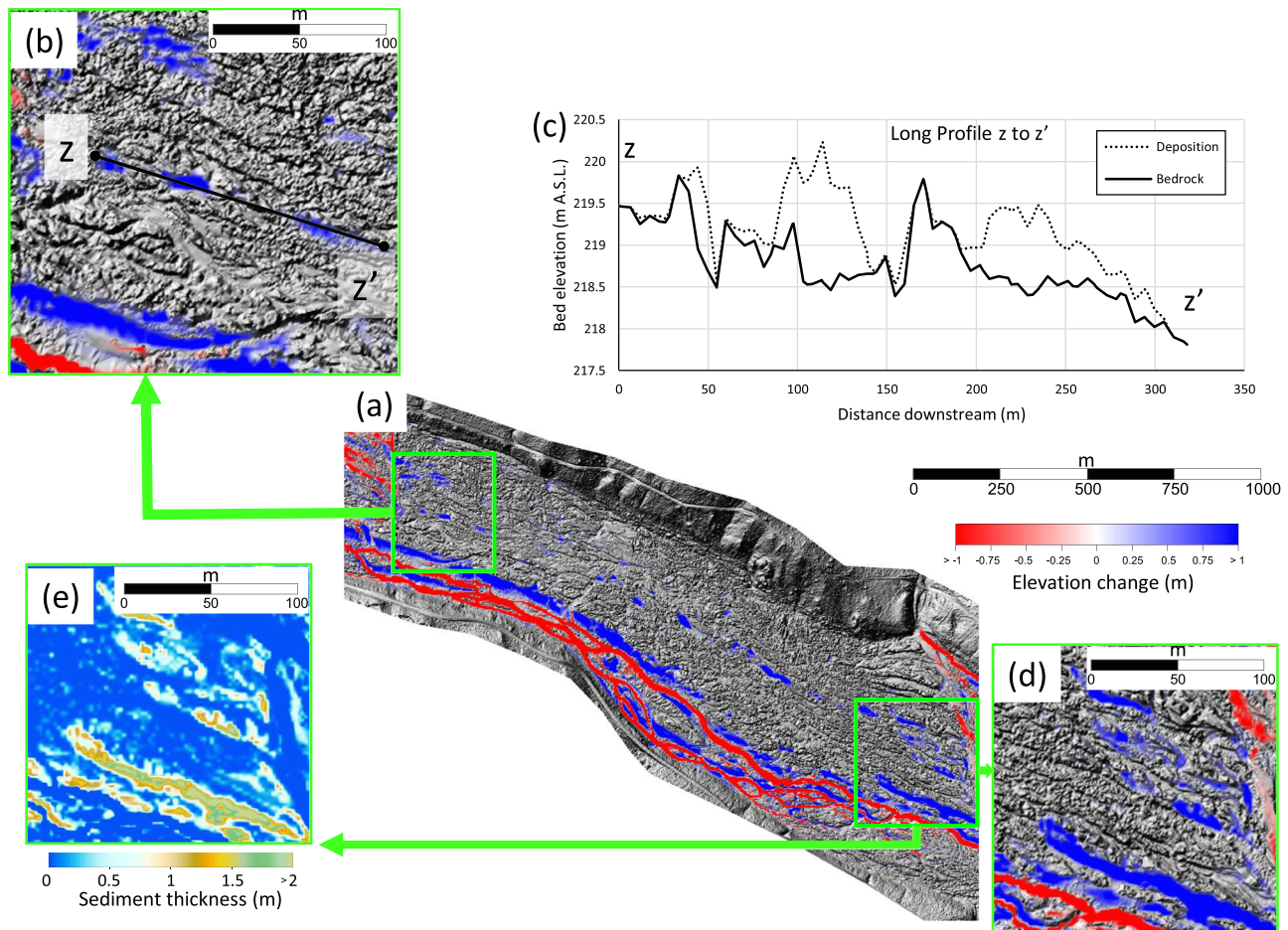


Figure 9. Erosion and deposition patterns after 52 hr of a simulated flood hydrograph in the bedrock anastomosed section of the study reach (for location, see orange shaded area in Figure 1b). (a) Simulated erosion and deposition. (b) Close-up showing deposition in topographic lows in the upstream part of the bedrock anastomosed section. The position of long profile $z-z'$ is indicated. (c) Long profile $z-z'$, illustrating a tendency for deposition in topographic lows. (d) Close-up showing deposition in topographic lows toward the downstream end of the bedrock anastomosed section. (e) DEM demonstrating that many areas of the simulated sediment deposits exhibit variable surface morphology, with higher interiors and lower margins.

The simulated patterns of geomorphic response presented in Figures 8b and 9 should be interpreted cautiously. As noted in section 3.3, the simulations were not designed to try and replicate the impacts of the Cyclone Dando floods but rather to provide insights into the possible topographic and hydraulic controls on erosion and deposition, especially over a stripped bedrock template. Indeed, the simulated results demonstrate the influence of local bedrock topographic lows on depositional patterns during waning flows (Figures 8b and 9), similar to what occurred in certain reaches during the Cyclone Dando floods (Figures 3c and 4a). Nonetheless, comparisons between the erosion and deposition patterns resulting from the 2012 floods (Figure 3b) and the patterns after 52 hr of the simulated flood (Figure 8b) also highlight some differences. For instance, following the simulated flood, erosion in the anabranches around the main area of islands at the upstream end of the study reach is less pronounced, and instead, there appears to be a linear ribbon of deposition along the southern edge of the area of islands (Figure 8b). More generally, throughout the study reach, the spatial extent of erosion and deposition following the simulated flood is less than occurred in response to the 2012 floods (compare Figures 3b and 8b). These differences may reflect limitations of the CAESAR-Lisflood model. CAESAR-Lisflood combines the CAESAR landscape evolution model with the Lisflood-LP reduced complexity flow model (Bates et al., 2010). Lisflood-LP is a one-dimensional inertial model derived from the full shallow water equations that is applied in x and y directions to simulate 2-D flow over a raster grid (Coulthard et al., 2013). Although CAESAR-Lisflood has the advantage of being far less computationally demanding in comparison to other computational fluid dynamic approaches that

use full or depth-averaged Navier–Stokes equations (e.g., Lane, 1998), it is a simple storage cell flow model that incorporates inertia, but only on a single-cell basis (Coulthard et al., 2013). As a result, more complex flow effects such as those found on the lee-side of bedrock highs and in topographic lows (e.g., eddies) are not simulated in the code. The observed differences may also reflect the reduced grid resolution (5 m) used in the simulations compared with the raw 1-m LiDAR data used to generate the DoD in Figure 3b. Although our simulated flood peak reflects the 2012 peak discharge, we had no information on hydrograph shape and hence flood duration, which could also explain some differences in erosion and deposition patterns. It was also not possible to simulate any variations in sediment supply that may have occurred over the 2012 floods (e.g., in relation to progressive erosion of alluvial reaches upstream and/or owing to sediment inputs from the Sand River tributary); instead, the morphodynamic simulations simply recirculated sediment within the model domain. Furthermore, CAESAR-Lisflood does not simulate vegetative effects, which add to the spatial variability of roughness and erosional resistance. These limitations notwithstanding, the simulated patterns of geomorphic response still help to generate insights into the possible hydraulic and topographic controls on erosion and deposition in the study reach, as explored further below.

4.4. Sediment Thickness Analysis Derived From Morphodynamic Simulations

Figure 10a shows the simulated sediment thicknesses for deposition over the bedrock template in the bedrock anastomosed section versus the detrended elevation, as obtained at various time intervals throughout the 52-hr CAESAR-Lisflood morphodynamic simulation. The results show negligible sedimentation early in the model run but clear, albeit localized, deposition on topographic highs during the flood peak and at elevated discharges on the falling limb. At the end of the model run, there appears to have been a change in the loci of sedimentation, with greatest sediment thicknesses found over intermediate-topography areas (0- to 1-m elevation), and in topographic lows (0- to –2-m elevation). Topographic highs (>1-m elevation) remain relatively sediment free. The lowest topography areas (–2- to –3-m elevation)—many of which represent the main channels—also remain relatively sediment free. Closer analysis of the DEM reveals that many areas of deposition approximate bar and island forms, with evidence of more elevated interiors and sharp breaks of slope at their margins (e.g., Figure 9e).

4.5. Topographic Controls on Velocity Patterns

To further investigate the controls on sediment transport and deposition, the relationship between topography and simulated depth-average velocities was investigated for various time intervals throughout the simulated flood hydrograph by extracting local topographic and velocity data from the CAESAR-Lisflood outputs for each wet pixel of the bedrock area (Figure 10b). The threshold velocities for motion of 2-mm particles (very coarse sand/granule size class boundary), based upon the Hjulström (1935) curve, are indicated by the stippled lines (Figure 10b). At peak flow discharge ($\sim 4,500 \text{ m}^3 \text{ s}^{-1}$), most topographic highs (>1-m elevation) are submerged. Velocities are widely in excess of the threshold throughout the reach but remain lower than the threshold over some topographic highs (Figure 10b; 7 hr). These zones of low-velocity flow enable localized deposition and so sediment thicknesses are greatest over topographic highs at this discharge (Figure 10a; 7 hr). By contrast, at peak discharge, some of the highest velocities are found in intermediate- and low-topography areas (1- to –1-m elevation); these areas are thus least likely to accumulate sediment but provide high rates of sediment throughput to lower topography areas (–1- to –3-m elevation) downstream. At $1,844 \text{ m}^3 \text{ s}^{-1}$, more than 50% of the velocities in the highest-topography areas (2- to 3-m elevation) tend to be below the threshold, so deposition on in these areas is enhanced, with sediment thicknesses increasing further (Figures 10a and 10b; 8 hr). At $954 \text{ m}^3 \text{ s}^{-1}$, the highest-topography areas (2- to 3-m elevation) tend to become exposed above the water surface but the lower tails of the box and whisker plots for the velocities at 0- to 1- and 1- to 2-m elevations are below the threshold, also resulting in some deposition, especially at 1- to 2-m elevation (Figures 10a and 10b; 9 hr). At 52 hr, however, there is no evidence of substantive sediment cover on the topographic highs (>1-m elevation), suggesting that much of the previously deposited sediment has been reworked during falling stage or by the smaller secondary flood peak of $410 \text{ m}^3 \text{ s}^{-1}$ at 33 hr. At discharges of $100 \text{ m}^3 \text{ s}^{-1}$, areas >1 m in elevation tend to be exposed, and flow velocities indicate that deposition is most likely to take place in intermediate- or low-topography areas (1- to –2-m elevation), corroborating the sediment thickness data (Figures 10a and 10b; 52 hr). At these low discharges, little

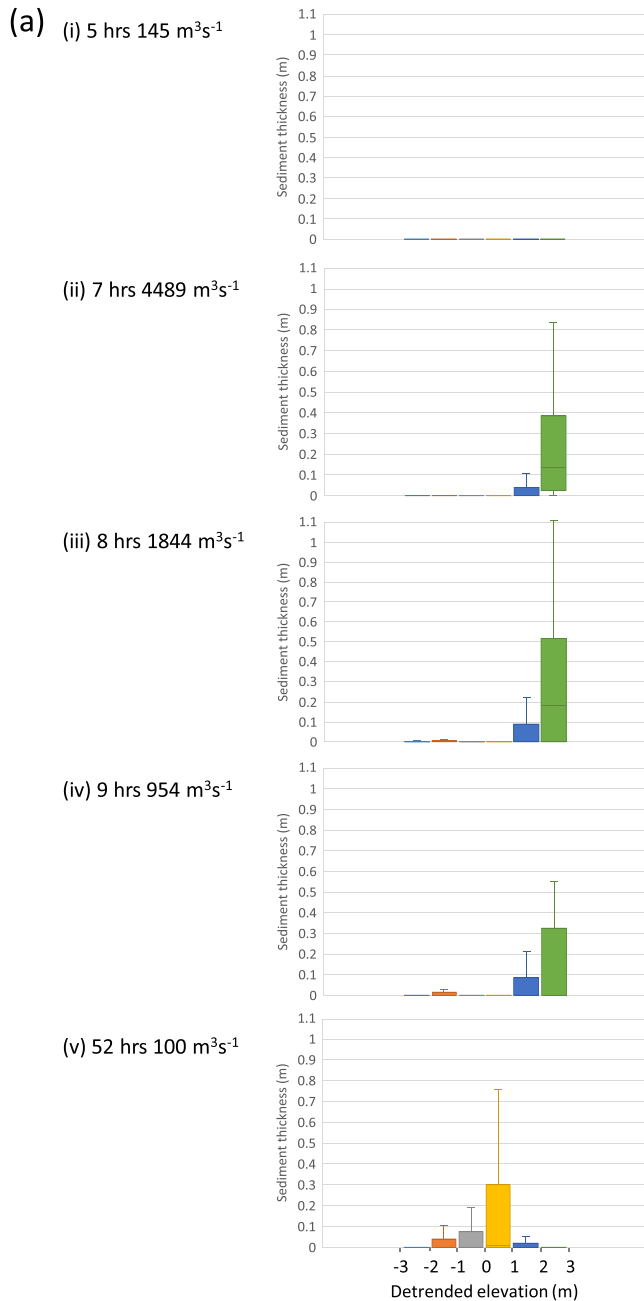


Figure 10. Box and whisker plots based on the results of simulated deposition in the bedrock anastomosed section of the study reach (Figure 1b). (a) Simulated sediment thicknesses for each pixel with sediment cover versus detrended elevation classes at intervals through the CAESAR-Lisflood run. (b) Simulated depth-averaged velocities for each wet pixel versus detrended elevation classes at different discharges. The dotted line on the plots represents the threshold velocity for motion of 2-mm particles (based on Hjulström, 1935).

deposition takes place in the lowest-topography areas (−2- to −3-m elevation) where the flow is concentrated (Figure 10a). In summary, at higher discharges, localized deposition tends to occur mainly on topographic highs. At lower discharges, topographic highs are not submerged, and so deposition becomes more likely in some of the intermediate- and low-elevation areas, especially in areas of waning flow; for example, bedrock anabranches that become increasingly disconnected from the main (deeper) bedrock channels as flow stage falls. Sand may still be mobile, particularly along the lowest-elevation areas (i.e., deeper bedrock channels that carry perennial flows), but with further decreases in discharge (e.g., $<100 \text{ m}^3 \text{ s}^{-1}$) the potential for more widespread, albeit temporary, deposition will increase.

5. Interpretation

Previous conceptual models of bar and island development for the mixed bedrock-alluvial, multichannel rivers of the KNP have assumed that deposition is initiated on topographic highs, which then continue to accumulate sediment and become vegetated (Rountree et al., 2000; van Niekerk et al., 1999). Our findings, however, suggest that these previous conceptual models need refinement, particularly by giving greater acknowledgment to the role of deposition over local topographic lows in the bedrock template as a precursor to bar and island growth.

Visual interrogation of the LiDAR DoD for the bedrock anastomosed section of the reach shows some evidence of deposition in topographic lows at the upstream end of the bedrock anastomosed area in response to the 2012 floods (Figures 3c and 4a). This finding is further supported by the LiDAR DoDs over more alluvial areas (e.g., mature bedrock-core bars at sites A and B) that were stripped in the 2012 floods, which tend to indicate thicker sediments over bedrock topographic lows (Figures 5–7). Our morphodynamic simulations suggest that while some initial deposition may occur on the highest-elevation areas during peak discharges, with falling stage and lower discharges some redistribution of sediment from these highs may occur, supporting a general tendency for deposition to become more widespread in intermediate-elevation and lower elevation areas (Figures 8–10). Our field surveys of the Sabie and other KNP rivers following the 2012 floods also revealed numerous instances of sandy deposits immediately adjacent to bedrock highs (see Milan, Heritage, Entwistle, et al., 2018, their Figure 5), suggesting that rainwash in the intervals between floods may also contribute to the small-scale reworking of sediment from local topographic highs into lower elevation areas (cf. the processes described by Gurnell et al., 2008). The lowest-elevation areas, which serve as perennial channels and convey flow over the full range of the flow regime, remain relatively free of sediment.

Deposition in these intermediate-elevation and lower elevation areas is thus likely to be fundamental to the initial development of bedrock-core bars in the early stages of reach-scale sediment accumulation following flood stripping events. Field observations, however, suggest that topographic and hydraulic controls offer only a partial explanation for bedrock-core bar development. The sediment that accumulates in topographic lows tends to have a higher moisture and organic content, and consequently may provide preferential niches for vegetation establishment.

On the Sabie and other KNP rivers, early successional vegetation types such as *B. salicina*, *Phragmites mauritianus*, and *Phyllanthus reticulatus*, which are able to establish

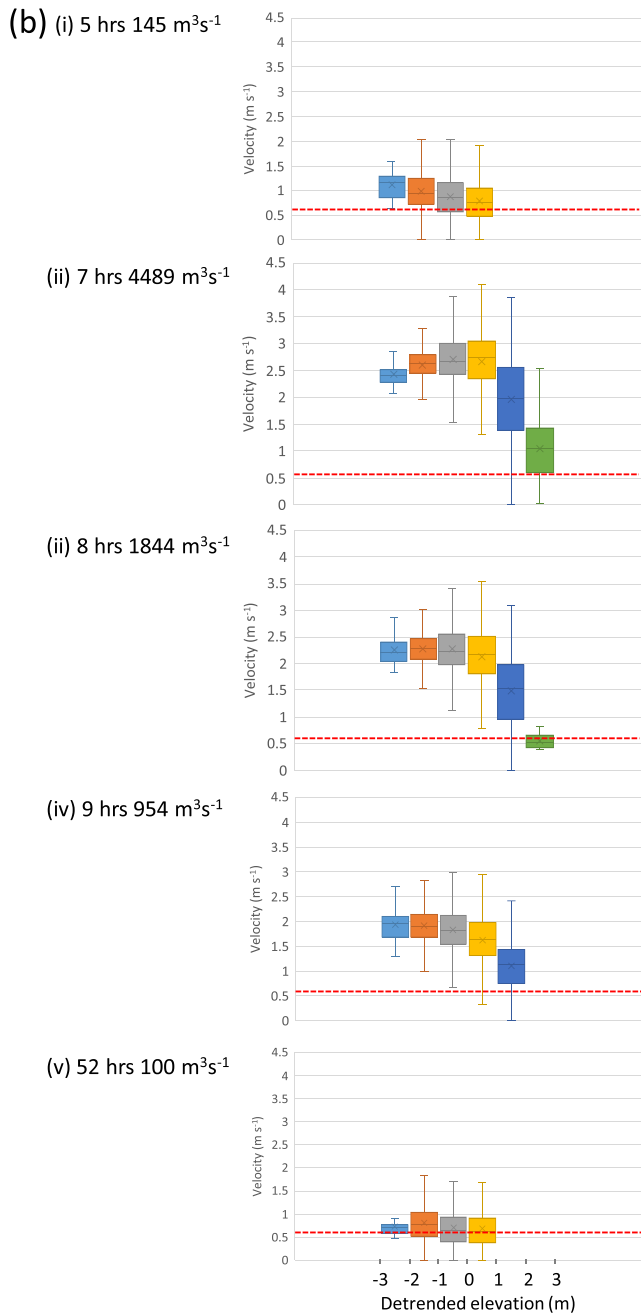


Figure 10. (continued)

Gurnell et al., 2008). Sediment is also routed in between the bedrock topographic highs during floods, and some deposition occurs in areas of lower velocity; for example, on the lee side of bedrock highs (Stage 2). The sediment rapidly becomes colonized by pioneer vegetation (e.g., *B. salicina*, *P. mauritianus*). Over time, floods may deliver more sediment to the lower elevation areas, which tend to retain more moisture and organic material, and so may be further colonized by other shrub species (e.g., *P. reticulatus*) and eventually some tree species (e.g., *Combretum erythrophyllum*; Stages 3 and 4). The vegetation has the effect of increasing erosional resistance, and as succession proceeds, plant structures are able to capture more sediment, propagules, and other organic material during floods (Stage 5). Given a sequence of low to moderate floods, this “building phase” may continue, with thicker sediment that hosts late successional plant species

in cracks in bedrock or can colonize rapidly on shallow substrates and lay down horizontal runners, are known to enhance sediment erosional resistance (van Coller et al., 1997). Vegetation establishment also helps to trap sediment and propagules supplied from upstream or from nearby isolated remnant vegetated sediment, leading to more sediment accumulation and establishment of reed and shrub/tree species, which in turn further enhances erosional resistance through the development of root structures. Later vegetation succession (e.g., by species such as *Combretum* spp. and *Syzygium guineense*) further stabilizes the deposits and captures additional sediment and propagules and other organic material during floods. For instance, large wood piles are commonly observed after large floods along the KNP rivers, and are known to be important in creating regeneration niches for riparian woodland on the Sabie River (Pettit & Naiman, 2006). In summary, we suggest that vegetation establishment and successional development is key to the development of a bedrock-core bar as (1) roots stabilize the sediment, increasing erosional resistance, and (2) reeds, shrubs, and trees increase hydraulic roughness and capture additional sediment, propagules, and other organic material, further enhancing local deposition and conditions for vegetation growth.

6. Discussion

The findings presented in this paper have been derived from a combination of aerial image analyses, morphodynamic simulations, and field investigations. Although focused on an ~4-km study reach of the Sabie River, alongside our previous studies of a more extensive reach of the middle Sabie River (Milan, Heritage, Tooth, et al., 2018) and other hydrologically and morphologically similar KNP rivers (e.g., Heritage et al., 2019; Milan, Heritage, Entwistle, et al., 2018), the results and interpretations provide new insights into the topographic, hydraulic, and vegetative controls on bar and island development, enabling us to challenge some previous conceptual models. In the following sections, we present a new conceptual model of bar and island growth for the KNP rivers, make comparisons with models of bar and island growth in other rivers, and discuss the wider significance of the findings for enhancing our knowledge of the dynamics of bedrock-influenced, multichannel rivers.

6.1. A New Conceptual Model for Bedrock-Core Bar and Island Development

Figure 11 presents a six-stage model of bar and island development in a mixed bedrock-alluvial, multichanneled reach of a KNP river. Following a flood stripping event, bedrock topographic highs are exposed and topographic lows are inundated (Stage 1). Sediment initially deposited on topographic highs during floods gets reworked into lower elevation areas on the falling limb of flood hydrographs or by subsequent rainwash (cf.

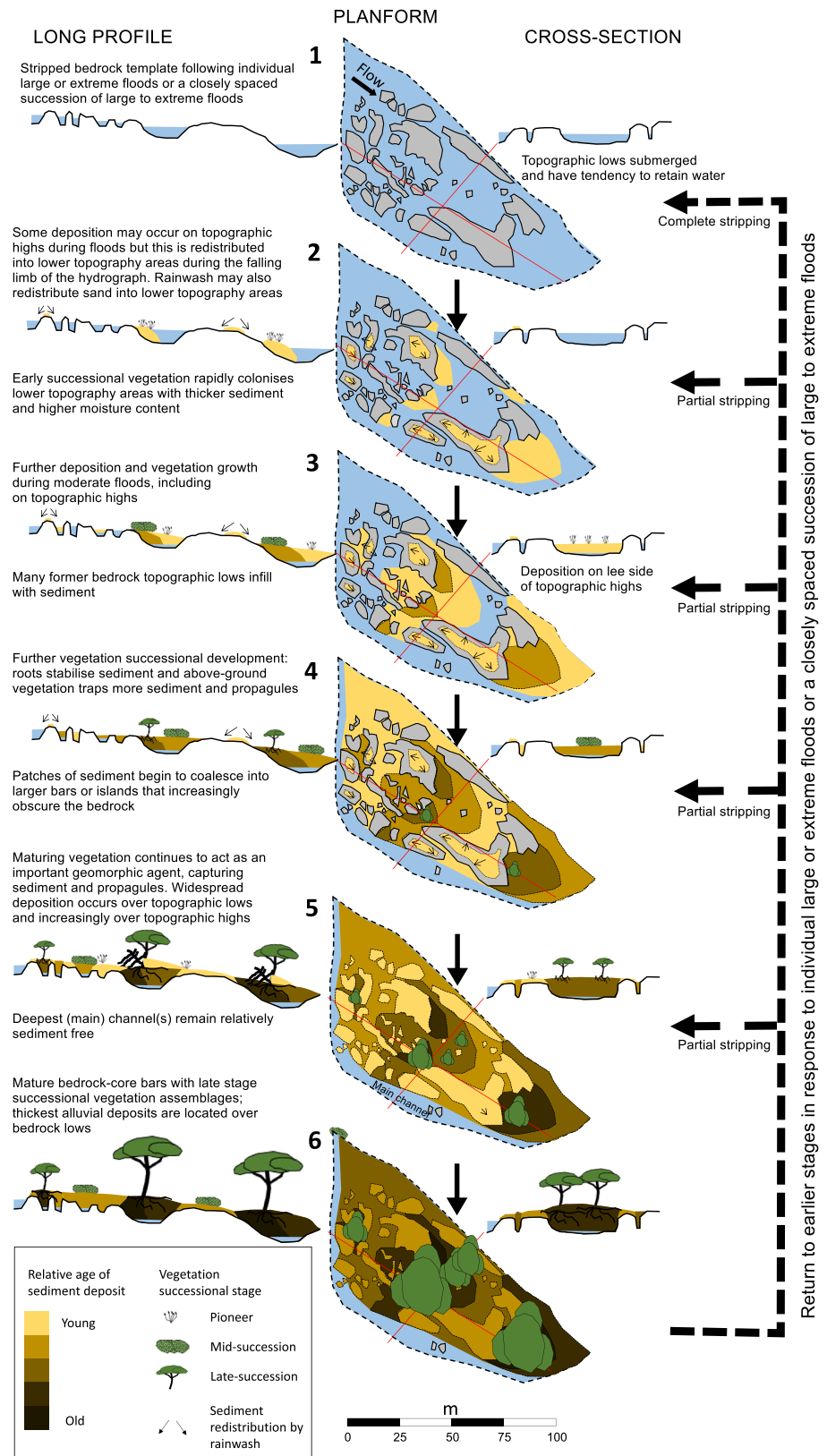


Figure 11. Conceptual model of bedrock-core bar and island development in mixed bedrock-alluvial, multichanneled rivers.

(bedrock-core bars and islands) ultimately being positioned over the initial topographic lows on the bedrock template (Stage 6). The more extensive the coverage of alluvium and vegetation, the greater the masking of the bedrock template is, with only the major topographic lows (deepest channels) now remaining free of sediment. This enhances the protective cover effect, with minor bedrock abrasion being focused along the deepest channels but with reduced rates of bedrock abrasion across the wider macrochannel floor (cf. Lague, 2014; Nelson & Seminara, 2011; Sklar & Dietrich, 2004). Large or extreme floods, however, may remove vegetation and erode alluvium; depending upon flow magnitude and sequencing, partial or full stripping can widely expose the underlying bedrock template (Figure 11) and result in more widespread bedrock erosion. Preliminary luminescence ages for alluvium from some of the KNP rivers suggest that historically the more extensive stripping events have tended to occur on multidecadal to centennial time scales (Heritage et al., 2014). Essentially, as Milan, Heritage, Tooth, et al. (2018) have outlined, along these supply-limited, flood-prone river systems, alluvial sediments are only in temporary storage, and with every stripping episode, some bedrock erosion will occur. The wide vertical and horizontal joint spacings (typically >0.5 m) in the gneisses and leucogranites that underlie much of the study reach tend to preclude extensive hydraulic plucking, and so in any individual flood, bedrock lowering is likely to be negligible (i.e., millimeter-scale). Nevertheless, through incremental bedrock erosion over many successive floods, rivers such as the Sabie will continue to etch their macrochannels into the landscape, thereby contributing to overall landscape denudation.

6.2. Comparison to Models of Bar and Island Growth in Other Rivers

Most previous studies of bar and island development have focused upon fully alluvial, perennial rivers, and have highlighted a variety of mechanisms for the initiation of depositional features such as bars and islands, including reductions in flow competence leading to sediment stalling (e.g., Ashmore, 1991; Ashworth, 1996; Dos Santos et al., 2017; Leli et al., 2018), sedimentation around organic debris (Gurnell et al., 2008; Gurnell & Petts, 2006; Nanson & Hickin, 1986), and accretion at the junction with tributaries (Jenkins, 2007). Additional island formation processes are outlined in overviews by Osterkamp (1998) and Wyrick and Klingeman (2011). Significantly, in these perennial rivers, vegetation (e.g., grasses, shrubs, trees) can be a crucial factor contributing to bar/island stabilization and growth but tends to respond to sedimentation, typically only colonizing bars and islands that are sufficiently elevated to be protected from regular inundation (e.g., Gurnell, 2014; Hupp, 1990; Hupp & Osterkamp, 1996; Nanson & Beach, 1977). By contrast, in rivers that are dry year-round or seasonally (ephemeral or intermittent rivers), even woody vegetation such as shrubs and trees can establish on channel beds and so can directly initiate the formation of depositional features such as bars, benches, ridges, and islands (e.g., Fielding et al., 1997; Graf, 1978; Hadley, 1961; Pickup et al., 1988; Woodyer et al., 1979). In some cases, this promotes extensive alluvial anabranching, as has been documented for many parts of dryland Australia (Tooth et al., 2008; Tooth & Nanson, 1999, 2000; Wende & Nanson, 1998). In these anabranching channels, some bars and islands may also form by dissection of once-continuous larger island or floodplain surfaces (Tooth & Nanson, 1999, 2000; Tooth et al., 2008; for a Namibian example, see Ringrose et al., 2018).

By comparison with these studies of alluvial rivers, bar and island development in mixed bedrock-alluvial, multichanneled rivers has received far less research attention. Outside of previous work in the KNP, exceptions include studies of the Orange River in South Africa and the Mekong River in northern Cambodia (Meshkova & Carling, 2012, 2013; Tooth & McCarthy, 2004), although the emphasis in these studies has tended to be more on documenting reach-scale controls on erosion and deposition and the associated channel pattern morphometrics, rather than on developing a process-based understanding of bar and island development. Our study of bar/island development thus adds significantly to previous research, particularly because the KNP rivers are characterized by an unusual combination of flow and sediment regimes. Rivers such as the Olifants (Milan, Heritage, Entwistle, et al., 2018) and the Sabie (this study) have perennial flow regimes, but during winter low flows and/or following large or extreme summer floods, large areas of the bedrock template in the macrochannel floor are exposed for extended periods. While few vegetation species can establish directly on the bedrock, even relatively minor sedimentation in bedrock lows provides conditions sufficient to support the establishment of pioneer vegetation (e.g., *P. mauritanus*). During sequences of low to moderate floods, sedimentation and vegetation growth can continue, with initial bedrock topographic lows becoming infilled, and adjacent depositional features coalescing to create larger bars and islands that

ultimately become topographic highs in the macrochannel (Figure 11). While our findings challenge the assumption of near-uniform, ubiquitous sedimentation on bedrock highs that underpins previous conceptual models of island development in the KNP rivers (Rountree et al., 2000; van Niekerk et al., 1999), the end result is similar. Following widespread stripping events, and under a scenario of successive low to moderate floods, sedimentation and vegetation establishment leads to a cycle of bar/island growth and vegetation succession that adds considerable geomorphological, sedimentary, and ecological diversity to the riverine corridor.

6.3. Wider Significance of Findings

Although detailed studies have yet to be undertaken, our new model of bar/island growth (Figure 11) may be more widely applicable. Many other rivers across southern Africa and farther afield are mixed bedrock-alluvial in character (Tooth, 2013), with many supporting extensive, dominantly alluvial anastomosing/anabranching reaches developed atop bedrock template (see the compilation in Tooth & McCarthy, 2004; see also Meshkova & Carling, 2012). Many of these rivers are characterized by highly variable flow regimes, with extended periods of low to moderate floods being interspersed by large or extreme floods that commonly lead to partial or complete stripping. Notwithstanding the different vegetation assemblages in these rivers, following stripping episodes, it is possible that alluvial bar/island initiation and growth on exposed bedrock templates results from similar processes of sedimentation and vegetation succession to that in the KNP rivers. In essence, our model (Figure 11) can be seen as a hypothesis that can be tested in future studies of mixed bedrock-alluvial, multichanneled rivers. Particular attention could be directed toward whether there are any differences in the processes and patterns of bar/island growth that could be attributed to particular vegetation species or communities, especially where vegetation compositions and distributions are changing as a result of human modification of flow regimes and/or the spread of exotic, invasive species (e.g., Blanchon & Bravard, 2007; Dean & Schmidt, 2011; Douglas et al., 2018). More widespread application of geochronology (e.g., luminescence dating, radiocarbon) will help to provide greater insight into the rates and time scales of bar and island development that occurs during building phases, particularly where these occur on multidecadal to centennial time scales (cf. Tooth et al., 2008; Ramirez et al., 2019).

7. Conclusions

A combination of aerial image analyses, 2-D morphodynamic simulations, and field data has provided new insights into bar and island development along the mixed bedrock-alluvial, multichannel Sabie River in the KNP, eastern South Africa. Contrary to the assumption of near-uniform, ubiquitous sedimentation on bedrock topographic highs that underpins previous conceptual models, our data suggest that bedrock-core bars and islands develop as a result of preferential sedimentation in local bedrock topographic lows. Sedimentation occurs as a result of deposition during waning flows, particularly in areas of the macrochannel floor that become disconnected from the main channels during falling stage. Rainwash may also contribute to local sediment redistribution between floods by reworking sediment initially deposited on topographic highs into lower elevation areas. The sediment that accumulates in lower elevation areas tends to have a higher moisture and organic content, and consequently provides preferential niches for vegetation establishment. Along the Sabie River and other similar rivers within the KNP, we suggest that vegetation establishment and successional development is key to the development of bedrock-core bars as (1) roots stabilize the sediment and increase erosional resistance and (2) reeds, shrubs, and trees are able to capture additional sediment, propagules, and other organic material, further enhancing local deposition and conditions for vegetation growth. Over time, these bars may grow vertically, longitudinally, and laterally, locally coalescing with neighboring bars or islands to form larger alluvial features.

Our model of bar and island development in the rivers of the KNP complements and extends previous studies of the processes and patterns of bar/island development in alluvial and especially mixed bedrock-alluvial, multichannel rivers. The model can serve as a hypothesis to be tested in further work on other mixed bedrock-alluvial, multichannel rivers across southern Africa and farther afield. Potentially fertile lines of enquiry may involve investigations of whether there are perceptible differences in the role played by natural and invasive, exotic vegetation species, and establishing comparative rates and time scales of bar and island growth. In an era of rapid environmental changes, when there is increasing concern over the

profound changes to many aspects of riverine ecosystem services resulting from changes to flood magnitude and frequency and flood sequencing (Milan, Heritage, Tooth, et al., 2018), such knowledge may help to support the development of improved management, conservation, and/or restoration strategies for these types of rivers.

Acknowledgments

This project was funded through the Natural Environment Research Council (NERC) Urgency grant NE/K001132/1. We would like to thank SANParks for supporting this research. The LiDAR data obtained through this funding are described in Milan, Heritage, and Tooth (2018) and available at <http://catalogue.ceda.ac.uk/uuid/a2e82c7f92dc4f389a7fb7e4e6629c9e>. The paper was improved through the supportive comments of three anonymous reviewers and the evaluation of the Associate Editor (F. Comiti) and Editor (E.E. Wohl).

References

- Ashmore, P. E. (1991). How do gravel-bed rivers braid? *Canadian Journal of Earth Sciences*, 28(3), 326–341. <https://doi.org/10.1139/e91-030>
- Ashworth, P. J. (1996). Mid-channel bar growth and its relationship to local flow strength and direction. *Earth Surface Processes and Landforms*, 21(2), 103–123. [https://doi.org/10.1002/\(SICI\)1096-9837\(199602\)21:2<103::AID-ESP569>3.0.CO;2-O](https://doi.org/10.1002/(SICI)1096-9837(199602)21:2<103::AID-ESP569>3.0.CO;2-O)
- Baggs Sargood, M., Cohen, T. J., Thompson, C. J., & Croke, J. (2015). Hitting rock bottom: Morphological responses of bedrock-confined streams to a catastrophic flood. *Earth Surface Dynamics*, 3(2), 265–279. <https://doi.org/10.5194/esurf-3-265-2015>
- Baker, V. (1977). Stream-channel response to floods, with examples from central Texas. *Geological Society of America Bulletin*, 88, 1057–1071. [https://doi.org/10.1130/0016-7606\(1977\)88<1057:SRTFWE>2.0.CO;2](https://doi.org/10.1130/0016-7606(1977)88<1057:SRTFWE>2.0.CO;2)
- Bates, P. D., Horritt, M. S., & Fewtrell, T. J. (2010). A simple inertial formulation of the shallow water equations for efficient two-dimensional flood inundation modelling. *Journal of Hydrology*, 387, 33–45. <https://doi.org/10.1016/j.jhydrol.2010.03.027>
- Blanchon, D., & Bravard, J. P. (2007). La stabilité des formes fluviales de l'Orange, entre variabilité naturelle et impacts des grands barrages (secteur Boegoeberg-Augrabies, Afrique du Sud). *Géographie Physique et Quaternaire*, 61, 21–37. <https://doi.org/10.7202/029568ar>
- Broadhurst, L.J., Heritage, G.H., van Niekerk, A.W., James, C.S., & Rogers, K.H. (1997). Translating discharge into local hydraulic conditions on the Sabie River: An assessment of channel flow resistance. Report-Water Research Commission, 2. Water Research Commission, Pretoria, South Africa, K5/474/0/1. 190 p.
- Chatanantavet, P., & Parker, G. (2008). Experimental study of bedrock channel alluviation under varied sediment supply and hydraulic conditions. *Water Resources Research*, 44, W12446. <https://doi.org/10.1029/2007WR006581>
- Coulthard, T. J., Neal, J. C., Bates, P. D., Ramirez, J., Almeida, G. A., & Hancock, G. R. (2013). Integrating the LISFLOOD-FP 2D hydrodynamic model with the CAESAR model: Implications for modelling landscape evolution. *Earth Surface Processes and Landforms*, 38(15), 1897–1906. <https://doi.org/10.1002/esp.3478>
- Dean, D. J., & Schmidt, J. C. (2011). The role of feedback mechanisms in historic channel changes of the lower Rio Grande in the Big Bend region. *Geomorphology*, 126(3–4), 333–349. <https://doi.org/10.1016/j.geomorph.2010.03.009>
- Dos Santos, V. C., Stevaux, J. C., & Assine, M. L. (2017). Fluvial processes in attachment bars in the upper Paraná River, Brazil. *Revista Brasileira de Geomorfologia*, 18(3), 483–499. <https://doi.org/10.20502/rbg.v18i3.1135>
- Douglas, C. M., Cowlishaw, G., Harrison, X. A., Henschel, J. R., Pettorelli, N., & Mulligan, M. (2018). Identifying the determinants of tree distributions along a large ephemeral river. *Ecosphere*, 9, e02223. <https://doi.org/10.1002/ecs2.2223>
- Eden, S. A. (1937). *From Sabi Game Reserve to Kruger National Park*. London: Cassell and Co.
- Entwistle, N., Heritage, G. L., & Milan, D. J. (2018). Recent remote sensing applications for hydro and morphodynamic monitoring and modelling. *Earth Surface Processes and Landforms*, 43(10), 2283–2291. <https://doi.org/10.1002/esp.4378>
- Fielding, C. R., Alexander, J., & Newman-Sutherland, E. (1997). Preservation of in situ, arboresecent vegetation and fluvial bar construction in the Burdekin River of North Queensland, Australia. *Palaeogeography, Palaeoclimatology, Palaeoecology*, 135(1–4), 123–144. [https://doi.org/10.1016/S0031-0182\(97\)00022-9](https://doi.org/10.1016/S0031-0182(97)00022-9)
- Finnegan, N. J., Sklar, L. S., & Fuller, T. K. (2007). Interplay of sediment supply, river incision, and channel morphology revealed by the transient evolution of an experimental bedrock channel. *Journal of Geophysical Research*, 112, F03S11. <https://doi.org/10.1029/2006JF000569>
- Fitchett, J. M., & Grab, A. W. (2014). A 66-year tropical cyclone record for south-east Africa: temporal trends in a global context. *International Journal of Climatology*, 34(13), 3604–3615. <https://doi.org/10.1002/joc.3932>
- Fitchett, J. M., Hoogendoorn, G., & Swemmer, A. M. (2016). Economic costs of the 2012 floods on tourism in the Mopani district municipality, South Africa. *Transactions of the Royal Society of South Africa*, 71(2), 187–194. <https://doi.org/10.1080/0035919X.2016.1167788>
- Goode, J. R., & Wohl, E. (2010). Coarse sediment transport in a bedrock channel with complex bed topography. *Water Resources Research*, 46, W11532. <https://doi.org/10.1029/2009WR008135>
- Graf, W. L. (1978). Fluvial adjustments to the spread of tamarisk in the Colorado Plateau region. *Geological Society of America Bulletin*, 89(10), 1491–1501. [https://doi.org/10.1130/0016-7606\(1978\)89<1491:FATTSO>2.0.CO;2](https://doi.org/10.1130/0016-7606(1978)89<1491:FATTSO>2.0.CO;2)
- Graf, W. L. (1983). The arroyo problem—Palaeohydrology and palaeohydraulics in the short term. In K. J. Gregory (Ed.), *Background to Palaeohydrology: A Perspective*, (pp. 279–302). Chichester, UK: Wiley.
- Gurnell, A. M. (2014). Plants as river system engineers. *Earth Surface Processes and Landforms*, 39(1), 4–25. <https://doi.org/10.1002/esp.3397>
- Gurnell, A. M., Blackall, T. D., & Petts, G. E. (2008). Characteristics of freshly deposited sand and finer sediments along an island-braided, gravel-bed river: The roles of water, wind and trees. *Geomorphology*, 99(1–4), 254–269. <https://doi.org/10.1016/j.geomorph.2007.11.009>
- Gurnell, A. M., & Petts, G. (2006). Trees as riparian engineers: The Tagliamento river, Italy. *Earth Surface Processes and Landforms*, 31(12), 1558–1574. <https://doi.org/10.1002/esp.1342>
- Hadley, R. F. (1961). *Influence of riparian vegetation on channel shape, northeastern Arizona*. United States Geological Survey, *Professional Paper*, Vol. 424-C, 30–31.
- Hereford, R. (1984). Twentieth-century geomorphology and alluvial stratigraphy of the Little Colorado River, Arizona. *Geological Society of America Bulletin*, 95, 654–668. [https://doi.org/10.1130/0016-7606\(1984\)95<654:CAEPTG>2.0.CO;2](https://doi.org/10.1130/0016-7606(1984)95<654:CAEPTG>2.0.CO;2)
- Hereford, R. (1993). *Entrenchment and Widening of the Upper San Pedro River, Arizona, Special Paper*, (Vol. 282, p. 46). Boulder, Colorado: Geological Society of America.
- Heritage, G., Entwistle, N., Tooth, S., & Milan, D. (2014). Long-term controls on semi-arid river form: Evidence from the Sabie and Olifants Rivers. In Y. J. Xu, M. A. Allison, S. J. Bentley, A. L. Collins, W. D. Erskine, V. Golosov, A. J. Horowitz, & M. Stone (Eds.), *Sediment dynamics from the summit to the sea, IAHS Publication*, (Vol. 367, pp. 141–146). Wallingford, Oxfordshire, UK: International Association of Hydrological Sciences.

- Heritage, G. L., Entwistle, N., Milan, D. J., & Tooth, S. (2019). Quantifying and contextualising cyclone-driven, extreme flood magnitudes in bedrock-influenced dryland rivers. *Advances in Water Research*, *123*, 145–159. <https://doi.org/10.1016/j.advwatres.2018.11.006>
- Heritage, G. L., Large, A. R. G., Moon, B. P., & Jewitt, G. (2004). Channel hydraulics and geomorphic effects of an extreme flood event on the Sabie River, South Africa. *Catena*, *58*(2), 151–181. <https://doi.org/10.1016/j.catena.2004.03.004>
- Heritage, G. L., Milan, D. J., Large, A. R. G., & Fuller, I. (2009). Influence of survey strategy and interpolation model upon DEM quality. *Geomorphology*, *112*(3–4), 334–344. <https://doi.org/10.1016/j.geomorph.2009.06.024>
- Heritage, G. L., & van Niekerk, A. W. (1995). Drought conditions and sediment transport in the Sabie River. *Koedoe*, *38*(2), 1–9. <https://doi.org/10.4102/koedoe.v38i2.311>
- Heritage, G. L., van Niekerk, A. W., & Moon, B. P. (1999). Geomorphology of the Sabie River, South Africa: An incised bedrock-influenced channel. In A. J. Miller, & A. Gupta (Eds.), *Varieties of Fluvial Form*, (pp. 53–79). Chichester: Wiley.
- Hjulström, F. (1935). Studies of the morphological activity of rivers as illustrated by the river Fyris. *Bulletin Geological Institute Upsala*, *25*, 221–227.
- Hodge, R. A., & Hoey, T. B. (2016). A Froude-scaled model of a bedrock-alluvial channel reach: 2. Sediment cover. *Journal of Geophysical Research: Earth Surface*, *121*, 1597–1618. <https://doi.org/10.1002/2015JF003709>
- Hodge, R. A., Hoey, T. B., & Sklar, L. S. (2011). Bed load transport in bedrock rivers: The role of sediment cover in grain entrainment, translation and deposition. *Journal of Geophysical Research*, *116*, F04028. <https://doi.org/10.1029/2011JF002032>
- Howard, A. D. (1994). A detachment-limited model of drainage basin evolution. *Water Resources Research*, *30*(7), 2261–2285. <https://doi.org/10.1029/94WR00757>
- Huda, S. A., & Small, E. E. (2014). Modeling the effects of bed topography on fluvial bedrock erosion by saltating bed load. *Journal of Geophysical Research: Earth Surface*, *119*, 1222–1239. <https://doi.org/10.1002/2013JF002872>
- Hupp, C. R. (1990). Vegetation patterns in relation to basin hydrogeomorphology. In J. B. Thornes (Ed.), *Vegetation and Erosion*, (pp. 217–237). New York: Wiley.
- Hupp, C. R., & Osterkamp, W. R. (1996). Riparian vegetation and fluvial geomorphic processes. *Geomorphology*, *14*(4), 277–295. [https://doi.org/10.1016/0169-555X\(95\)00042-4](https://doi.org/10.1016/0169-555X(95)00042-4)
- Jenkins, P.A. 2007. Map-based tests on controls of anabranch river character on the lower Yellowstone River, unpublished Masters thesis, Montana State University
- Johnson, J. P., & Whipple, K. X. (2007). Feedbacks between erosion and sediment transport in experimental bedrock channels. *Earth Surface Processes and Landforms*, *32*(7), 1048–1062. <https://doi.org/10.1002/esp.1471>
- Johnson, J. P. L. (2014). A surface roughness model for predicting alluvial cover and bed load transport rate in bedrock channels. *Journal of Geophysical Research: Earth Surface*, *119*, 2147–2173. <https://doi.org/10.1002/2013JF003000>
- Kale, V. S., Baker, V. R., & Mishra, S. (1996). Multi-channel patterns of bedrock rivers: An example from the central Narmada basin, India. *Catena*, *26*(1–2), 85–98. [https://doi.org/10.1016/0341-8162\(95\)00035-6](https://doi.org/10.1016/0341-8162(95)00035-6)
- Knight, J., & Evans, M. (2017). The sediment stratigraphy of a flood event: An example from the Sabie River, South Africa. *Catena*, *151*, 87–97. <https://doi.org/10.1016/j.catena.2016.12.015>
- Lague, D. (2014). The stream power river incision model: Evidence, theory and beyond. *Earth Surface Processes and Landforms*, *39*(1), 38–61. <https://doi.org/10.1002/esp.3462>
- Lane, S. N. (1998). Hydraulic modelling in hydrology and geomorphology: A review of high resolution approaches. *Hydrological Processes*, *12*(8), 1131–1150. [https://doi.org/10.1002/\(SICI\)1099-1085\(19980630\)12:8<1131::AID-HYP611>3.0.CO;2-K](https://doi.org/10.1002/(SICI)1099-1085(19980630)12:8<1131::AID-HYP611>3.0.CO;2-K)
- Leli, I. T., Stevaux, J. C., & Assine, M. L. (2018). Genesis and sedimentary record of blind channel and islands of the anabranching river: An evolution model. *Geomorphology*, *302*, 35–45. <https://doi.org/10.1016/j.geomorph.2017.05.001>
- MacFadyen, S., Zambatis, N., van Teeffelen, A. J., & Hui, C. (2018). Long-term rainfall regression surfaces for the Kruger National Park, South Africa: A spatio-temporal review of patterns from 1981 to 2015. *International Journal of Climatology*, *38*(5), 2506–2519. <https://doi.org/10.1002/joc.5394>
- McCarthy, T. S., & Tooth, S. (2004). Incised meanders along the mixed bedrock-alluvial Orange River, northern Cape Province, South Africa. *Zeitschrift für Geomorphologie*, *48*(3), 273–292.
- Meshkova, L. V., & Carling, P. A. (2012). The geomorphological characteristics of the Mekong river in northern Cambodia: A mixed bedrock-alluvial multi-channel network. *Geomorphology*, *147–148*, 2–17. <https://doi.org/10.1016/j.geomorph.2011.06.041>
- Meshkova, L. V., & Carling, P. A. (2013). Discrimination of alluvial and mixed bedrock-alluvial multichannel river networks. *Earth Surface Processes and Landforms*, *38*(11), 1299–1316. <https://doi.org/10.1002/esp.3417>
- Milan, D., Heritage, G., Entwistle, N., & Tooth, S. (2018). Morphodynamic simulation of sediment deposition patterns on a recently stripped bedrock anastomosed channel. *Proceedings IAHS*, *377*, 51–56. <https://doi.org/10.5194/piahs-377-51-2018>
- Milan, D.J., Heritage, G., & Tooth, S. (2018). Kruger National Park Rivers LiDAR data (May 2012). Centre for Environmental Data Analysis, available at: <http://catalogue.ceda.ac.uk/uuid/a2e82c7f92dc4f389a7fb7e4e6629c9e>
- Milan, D. J., & Heritage, G. L. (2012). LiDAR and ADCP use in gravel bed rivers: Advances since GBR6. In M. Church, P. Biron, & A. Roy (Eds.), *Gravel-bed rivers: Processes, Tools, Environments*, (pp. 286–302). Chichester: John Wiley & Sons.
- Milan, D. J., Heritage, G. L., & Hetherington, D. (2007). Application of a 3D laser scanner in the assessment of erosion and deposition volumes in a proglacial river. *Earth Surface Processes and Landforms*, *32*(11), 1657–1674. <https://doi.org/10.1002/esp.1592>
- Milan, D. J., Heritage, G. L., Large, A. R. G., & Fuller, I. D. (2011). Filtering spatial error from DEMs: Implications for morphological change estimation. *Geomorphology*, *125*(1), 160–171. <https://doi.org/10.1016/j.geomorph.2010.09.012>
- Milan, D. J., Heritage, G. L., Tooth, S., & Entwistle, N. (2018). Morphodynamics of bedrock-influenced dryland rivers during extreme floods: Insights from the Kruger National Park, South Africa. *Geological Society of America Bulletin*, *130*(11–12), 1825–1841. <https://doi.org/10.1130/B31839.1>
- Moon, B. P., & Heritage, G. L. (2001). The contemporary geomorphology of the Letaba River in the Kruger National Park. *Koedoe*, *44*(1), 45–55.
- Nanson, G. (1986). Episodes of vertical accretion and catastrophic stripping: A model of disequilibrium floodplain development. *Geological Society of America Bulletin*, *97*(12), 1467–1475. [https://doi.org/10.1130/0016-7606\(1986\)97<1467:EOVAAAC>2.0.CO;2](https://doi.org/10.1130/0016-7606(1986)97<1467:EOVAAAC>2.0.CO;2)
- Nanson, G. C., & Beach, H. F. (1977). Forest succession and sedimentation on a meandering-river floodplain, northeast British Columbia, Canada. *Journal of Biogeography*, *4*(3), 229–251. <https://doi.org/10.2307/3038059>
- Nanson, G. C., & Hickin, E. J. (1986). A statistical analysis of bank erosion and channel migration in western Canada. *Geological Society of America Bulletin*, *97*(4), 497–504. [https://doi.org/10.1130/0016-7606\(1986\)97<497:ASAOBE>2.0.CO;2](https://doi.org/10.1130/0016-7606(1986)97<497:ASAOBE>2.0.CO;2)
- Nelson, P. A., & Seminara, G. (2011). Modeling the evolution of bedrock channel shape with erosion from saltating bed load. *Geophysical Research Letters*, *38*, L17406. <https://doi.org/10.1029/2011GL048628>

- Osterkamp, W. R. (1998). Processes of fluvial island formation, with examples from Plum Creek, Colorado and Snake River, Idaho. *Wetlands*, 18(4), 530–545. <https://doi.org/10.1007/BF03161670>
- Parsons, M., McLoughlin, C. A., Rountree, M. W., & Rogers, K. H. (2006). The biotic and abiotic legacy of a large infrequent flood disturbance in the Sabie River, South Africa. *River Research and Applications*, 22(2), 187–201. <https://doi.org/10.1002/rra.905>
- Pettit, N. E., & Naiman, R. J. (2006). Flood-deposited wood creates regeneration niches for riparian vegetation on a semi-arid South African river. *Journal of Vegetation Science*, 17(5), 615–624. <https://doi.org/10.1111/j.1654-1103.2006.tb02485.x>
- Pickup, G., Allan, G., & Baker, V. (1988). History, palaeochannels and palaeofloods of the Finke River, central Australia. In R. F. Warner (Ed.), *Fluvial geomorphology of Australia*, (pp. 177–200). Sydney: Academic Press.
- Ramírez, A. I. A., Rasbold, G. G., Parolin, M., & Stevaux, J. C. (2019). Phytoliths and seeds in fluvial island paleoenvironment reconstruction (interaction with pollen analysis). *Journal of South American Earth Sciences*, 89, 30–38. <https://doi.org/10.1016/j.jsames.2018.10.011>
- Ringrose, S., Seely, M., Matheson, W., Cassidy, L., Kemosidile, T., Diskin, S., & Coetzee, S. (2018). Nature and possible origins of hyper-arid floodplain islands: Exemplified by the Kuiseb River, Namibia. *Transactions of the Royal Society of South Africa*, 73(2), 143–157. <https://doi.org/10.1080/0035919X.2018.1435430>
- Rountree, M. W., Heritage, G. L., Rogers, K. H., & Acreman, M. C. (2001). In-channel metamorphosis in a semiarid, mixed bedrock/alluvial river system: Implications for instream flow requirements. In M. C. Acreman (Ed.), *Hydroecology: Linking Hydrology and Aquatic Ecology*, IAHS (Vol. 266, pp. 113–124). Wallingford, Oxfordshire, UK: International Association of Hydrological Sciences (IAHS).
- Rountree, M. W., Rogers, K. H., & Heritage, G. L. (2000). Landscape state change in the semi-arid Sabie River, Kruger National Park, in response to flood and drought. *South African Geographical Journal*, 82(3), 173–181. <https://doi.org/10.1080/03736245.2000.9713711>
- Sklar, L. S., & Dietrich, W. E. (2004). A mechanistic model for river incision into bedrock by saltating bed load. *Water Resources Research*, 40, W06301. <https://doi.org/10.1029/2003WR002496>
- Smithers, J. C., Schulze, R. E., Pike, A., & Jewitt, G. P. W. (2001). A hydrological perspective of the February 2000 floods: A case study in the Sabie River catchment. *Water SA*, 27(3), 325–332. <https://doi.org/10.4314/wsa.v27i3.4975>
- Tooth, S. (2013). Dryland fluvial environments: assessing distinctiveness and diversity from a global perspective. In Shroder, J. (Editor in Chief) and Wohl, E.E. (Ed.), *Treatise on Geomorphology*. Academic Press, San Diego, CA, Vol. 9, *Fluvial Geomorphology*, pp. 612–644 (DOI: <https://doi.org/10.1016/B978-0-12-374739-6.00257-8>).
- Tooth, S. (2016). Changes in fluvial systems during the Quaternary. In J. Knight, & S. Grab (Eds.), *Quaternary environmental change in southern Africa: Physical and human dimensions*, (pp. 170–187). Cambridge: Cambridge University Press.
- Tooth, S., Hancox, P. J., Brandt, D., McCarthy, T. S., Jacobs, Z., & Woodborne, S. (2013). Controls on the genesis, sedimentary architecture, and preservation potential of dryland alluvial successions in stable continental interiors: Insights from the incising Modder River, South Africa. *Journal of Sedimentary Research*, 83(7), 541–561. <https://doi.org/10.2110/jsr.2013.46>
- Tooth, S., Jansen, J. D., Nanson, G. C., Coulthard, T. J., & Pietsch, T. (2008). Riparian vegetation and the late Holocene development of an anabranching river: Magela Creek, northern Australia. *Geological Society of America Bulletin*, 120(7–8), 1021–1035. <https://doi.org/10.1130/B26165.1>
- Tooth, S., & McCarthy, T. S. (2004). Anabranching in mixed bedrock-alluvial rivers: The example of the Orange River above Augrabies Falls, Northern Cape Province, South Africa. *Geomorphology*, 57(3–4), 235–262. [https://doi.org/10.1016/S0169-555X\(03\)00105-3](https://doi.org/10.1016/S0169-555X(03)00105-3)
- Tooth, S., & Nanson, G. C. (1999). Anabranching rivers on the Northern Plains of arid central Australia. *Geomorphology*, 29(3–4), 211–233. [https://doi.org/10.1016/S0169-555X\(99\)00021-5](https://doi.org/10.1016/S0169-555X(99)00021-5)
- Tooth, S., & Nanson, G. C. (2000). The role of vegetation in the formation of anabranching channels in an ephemeral river, Northern plains, arid central Australia. *Hydrological Processes*, 14(16–17), 3099–3117. [https://doi.org/10.1002/1099-1085\(200011/12\)14:16/17<3099::AID-HYP136>3.0.CO;2-4](https://doi.org/10.1002/1099-1085(200011/12)14:16/17<3099::AID-HYP136>3.0.CO;2-4)
- Tooth, S., & Nanson, G. C. (2011). Distinctiveness and diversity of arid zone rivers. In D. S. G. Thomas (Ed.), *Arid Zone Geomorphology: Process, Form and Change in Drylands*, (3rd ed., pp. 269–300). Chichester: Wiley-Blackwell.
- van Coller, A., Rogers, K., & Heritage, G. L. (1997). Linking riparian vegetation types and fluvial geomorphology along the Sabie River within the Kruger National Park, South Africa. *African Journal of Ecology*, 35(3), 194–212. <https://doi.org/10.1111/j.1365-2028.1997.090-89090.x>
- van Niekerk, A. W., Heritage, G. L., Broadhurst, L. J., & Moon, B. P. (1999). Bedrock anastomosing channel systems: Morphology and dynamics in the Sabie River, Mpumalanga Province, South Africa. In A. J. Miller, & A. Gupta (Eds.), *Varieties of Fluvial Form*, (pp. 219–247). Chichester, UK: John Wiley and Sons, Ltd.
- van Niekerk, A. W., Heritage, G. L., & Moon, B. P. (1995). River classification for management: The geomorphology of the Sabie River. *South African Geographical Journal*, 77(2), 68–76. <https://doi.org/10.1080/03736245.1995.9713594>
- Wende, R., & Nanson, G. C. (1998). Anabranching rivers: Ridge-form alluvial channels in tropical northern Australia. *Geomorphology*, 22(3–4), 205–224. [https://doi.org/10.1016/S0169-555X\(97\)00085-8](https://doi.org/10.1016/S0169-555X(97)00085-8)
- Wilcock, P. R., & Crowe, J. C. (2003). Surface-based transport model for mixed-size sediment. *Journal of Hydraulic Engineering*, 129(2), 120–128. [https://doi.org/10.1061/\(ASCE\)0733-9429\(2003\)129:2\(120\)](https://doi.org/10.1061/(ASCE)0733-9429(2003)129:2(120))
- Woodyer, K. D., Taylor, G., & Crook, K. A. W. (1979). Sedimentation and benches in a very low gradient suspended load stream, the Barwon River, New South Wales. *Sedimentary Geology*, 22(1–2), 97–120. [https://doi.org/10.1016/0037-0738\(79\)90023-X](https://doi.org/10.1016/0037-0738(79)90023-X)
- Wyrick, J. R., & Klingeman, P. C. (2011). Proposed fluvial island classification scheme and its use for river restoration. *River Research and Applications*, 27(7), 814–825.